Quantification of lung damage after lung cancer treatment with radiation therapy

2011

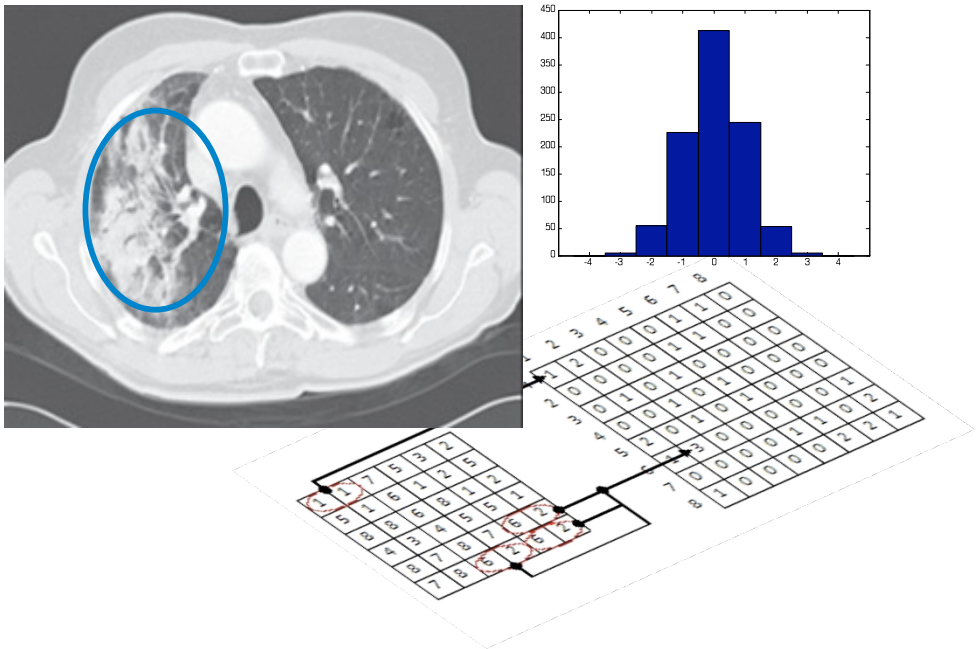

Biomedical Engineering 10th semester
Group 1086c

Christina Schel Klausen
Lone Nielsen

AALBORG UNIVERSITY

AALBORG UNIVERSITY

Department of Health Science and Technology
Fredrik Bajers Vej 7
9220 Aalborg
Denmark

Title: Quantification of lung damage after lung cancer treatment with radiation therapy

Theme: Applied biomedical engineering and informatics

Project period: 02.02.2011 – 01.06.2011

Project group: 10. sem., Group 1086c

Participants:

Christina S. Klausen

Lone Nielsen

Supervisors:

Lasse Riis Østergaard

Anne Sofie Korsager

Synopsis:
Lung cancer is the leading cause of cancer related deaths in the world and non-small cell lung cancer (NSCLC) is the most common type. In the diagnosis and treatment planning of NSCLC, computed tomography (CT) is often used as it excels in distinguishing tumours. Over 50 % of the patients receive radiation therapy (RT) during treatment. In RT, x-ray beams cause damage to the cancer cells by which they die or lose their ability to replicate. To compensate for e.g. patient movement, a larger area than the tumour is irradiated during RT. This may cause damage to normal tissue of the lungs. Acute pneumonitis occurs in 1-20 % of NSCLC patients three months after RT. In CT images, irregular consolidations of diffuse hazes will appear when pneumonitis is present. To grade such lung damage scoring systems exist. These do not provide an accurate assessment of lung damage, as they are inconsistent and do not entail enough detail. Hence, diagnosis is difficult and not very quantitative. The aim of this project is to develop a method enabling quantification of lung damage caused by NSCLC treatment with RT, using baseline and three month follow-up CT images. Sets of CT images from patients with/without lung damage were available. The methodology involves segmentation of the CT images to obtain the lungs and a texture analysis (TA) of the lung tissue. In the TA, texture features from an image histogram and a co-occurrence matrix were derived. The texture features were used to investigate whether they enable a differentiation between patients with/without lung damage. MINC, C programming, and MATLAB® were used for the image and data processing. Analysis and testing of the results were conducted by applying a MANOVA test and a discriminant analysis. A distinct differentiation between patients with/without lung damage could not be made with either the MANOVA test or the discriminant analysis. However, TA should not be disregarded in quantification of lung damage since several factors can be further investigated.

Copies: 6
Pages: 52
Attachments: None.
Finished: 01.06.2011

Preface

The report *Quantification of lung damage after lung cancer treatment with radiation therapy* is written at the Department of Health Science and Technology at Aalborg University by group 1086c on the 10th semester, Medical Informatics. The project period is from the 2nd of February 2011 to the 1st of June 2011.

The theme of this semester is *Applied biomedical engineering and informatics*. The aim of this project is to examine whether it is possible to develop a method which enables quantification of lung damage after lung cancer treatment with radiation therapy.

The project group would like to thank Jesper Carl, Chief Physicist at Dept. Medical Physics, Oncology, Aalborg Hospital South, Denmark, for providing data and good co-operation during the course of the project.

The project is supervised by Lasse Riis Østergaard and Anne Sofie Korsager.

Christina Schel Klausen

Lone Nielsen

Illustrations on front page are modified from [5] and [18].

Contents

1 Introduction **9**

2 Problem analysis **11**
2.1 Pathogenesis of lung cancer 11
2.1.1 Diagnosis and staging of lung cancer 12
2.2 Computed Tomography 13
2.2.1 History and principle of Computed Tomography 13
2.2.2 Acquisition of data 14
2.2.3 Image reconstruction 15
2.2.4 Quality of CT images 16
2.3 Treatment of lung cancer 16
2.3.1 Surgery 16
2.3.2 Chemotherapy 16
2.3.3 Radiation therapy 17

3 Problem statement **21**
3.1 Summary 21
3.2 Aim of the project 21

4 Presentation of methods for image analysis **23**
4.1 Segmentation of medical images 23
4.1.1 Threshold-based segmentation methods 24
4.1.2 Clustering-based segmentation methods 24
4.1.3 Deformable model-based segmentation methods 25
4.2 Texture analysis of medical images 26
4.2.1 Image histogram 26
4.2.2 Absolute gradient 27
4.2.3 Run-length matrix 27
4.2.4 Co-occurrence matrix 27
4.2.5 Texture analysis of volumetric data 28

5 Method for quantification of lung damage **31**
5.1 Description of data 31
5.2 Tools for visualisation and interaction with data 32
5.3 Segmentation of CT images 32
5.4 Texture analysis of CT images 35
5.5 Image histogram 35
5.5.1 Extraction of grey-level intensities 36

5.5.2 Texture features derived from image histogram-data 36
5.6 Co-occurrence matrix 37
5.6.1 Computation of co-occurrence matrix 38
5.6.2 Texture features derived from co-occurrence matrix 38

6 Evaluation of results **41**
6.1 Presentation of derived texture features 41
6.2 Theory of MANOVA 45
6.3 Application of MANOVA 46
6.4 Discriminant analysis for further evaluation of results 48
6.4.1 Classification of patients by discriminant analysis 49

7 Recapitulation **51**
7.1 Discussion 51
7.2 Conclusion 53

Bibliography **55**

Chapter 1

Introduction

Lung cancer is the leading cause of cancer related deaths in the world, and as of 2008 it is annually responsible for approximately 1.4 million deaths worldwide [25]. In the majority of cases the cause is related to smoking, and despite changes in smoking habits it remains a frequent cause of cancer related deaths. Other risk factors include among other passive smoking and asbestos. [9]
Cure of lung cancer is possible although the prognosis often is poor. Careful supervision of lung cancer may however extend life of the patient when cure is not possible. [9]

Lung cancer is a disease which involves an uncontrolled growth of abnormal cells in the tissues of the lung. [9] The uncontrolled growth of abnormal cells leads to formation of a malignant mass, which is named a tumour. Different types of lung cancer exist. Lung cancer is categorized based on where it has originated or spread from and which cells are involved. Primary lung cancer arises in the lungs and it is often carcinomas, i.e. invasive malignant tumours. Different carcinomas exist, but the most common type is non-small cell lung cancer (NSCLC) which accounts for about 80 % of all lung cancer cases [9]. Symptoms of lung cancer are often both vague and non-specific. As diagnosis of a disease relies on the recognition of symptoms, it can be difficult if a specific symptom like cough for lung cancer, is not present. The diagnosis of lung cancer often involves several different tests, e.g. radiographic ones. [9] [24] Computed Tomography (CT) is a medical image technique which is often used during diagnosis and the treatment planning of lung cancer. CT imaging provides cross-sectional images of the body by the means of x-radiation. X-radiation is composed of x-rays which can have energies which are able to penetrate human tissue. [20] In CT imaging, a narrow beam of x-rays is passed from an x-ray source through the patient. The x-rays are subsequently measured by an x-ray detector, and as the body consists of several types of tissue x-rays are absorbed in varying degrees. Hence, the imaging of anatomy is facilitated. The contrast resolution of CT imaging is best when compared to other medical imaging techniques using x-rays, and CT imaging excels in distinguishing soft tissue tumours. [10]

In treatment of lung cancer, different options exist and the type of treatment generally depends on the progress of the cancer. Surgery offers the best cure of lung cancer, but some patients may have additional diseases and thus become unqualified for surgery. Also, the tumour can be inoperable. [27] Over 50 % of the patients receive radiation therapy at some point during their treatment [9]. Radiation therapy seeks to damage cancer cells by target-

ing cancer with x-ray beams which cause the cells to die or lose their ability to replicate. [24] During radiation therapy, a larger area than the tumour is irradiated to compensate for patient movement, organ motion, and microscopic spread. Normal tissue in the lungs is thus affected as well, and it may result in side effects and damage to healthy cells. Acute pneumonitis occur in 1 % to 20 % of NSCLC patients three months after completion of radiation therapy, and it causes radiological changes in the field of irradiation [13]. In CT images, pneumonitis presents irregular consolidations of diffuse hazes. Such radiological changes can disappear but they may also lead to fibrous changes resulting in radiation fibrosis. Side effects of radiation therapy can be graded by using scoring systems. Although different scoring systems exist, they do not provide an accurate assessment of the side effects. The scoring systems do not entail enough detail and are not consistent for which reason the diagnosis becomes difficult and not very quantitative. [9] [6]

A method for quantifying radiation pneumonitis after lung cancer treatment with radiation therapy, is thus assumed to be beneficial. The aim of the following analysis is to:

Investigate whether radiation pneumonitis can be quantified using CT images, which are already used during diagnosis and the treatment planning of lung cancer.

Chapter 2

Problem analysis

In this chapter, the pathogenesis of lung cancer will be presented, followed by a description of the diagnosis of lung cancer. Afterwards, Computed Tomography (CT) is presented due to its use in the diagnosis and lung cancer treatment. Potential side effects from lung cancer treatment are also described.

2.1 Pathogenesis of lung cancer

Lung cancer is similar to numerous other cancers initiated by activation of oncogenes, which are genes that may cause cancer or inactivation of tumour suppressor genes. [12] In development of cancer, normal cells are transformed into cancer cells. A progression of changes on the cellular and genetic level occurs and leads to reprogramming of cells to undergo an uncontrolled cell division. Hence, a growth of abnormal cells occurs and thereby a malignant mass, i.e. a tumour, is formed. [9] [24] In Figure 2.1, a CT image of a tumour in the lung is seen. The tumour is indicated with the red arrow in the figure.

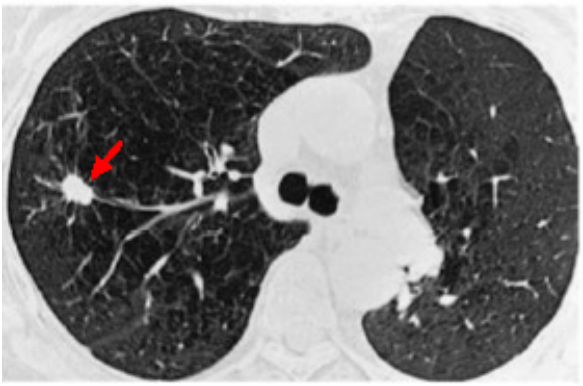

Figure 2.1: The figure shows a CT image of a NSCLC tumour, where the tumour is indicated with a red arrow. [7]

Lung cancer can be primary or secondary. Primary lung cancer is cancer which arises in the lungs, whereas cancer which has spread from other organs to the lungs is entitled secondary. The majority of primary lung cancers are carcinomas. Carcinoma refers to an invasive

malignant tumour which is derived from epithelial cells. Primary lung cancer is broadly divided into non-small cell lung cancer (NSCLC) and small cell lung cancer (SCLC). The devision into NSCLC and SCLC is based on the involved type of cell, the treatment, and the prognosis. Overall SCLC has a worse prognosis than NSCLC. NSCLC is the most common as it accounts for approximately 80 % of all lung cancer cases [9]. NSCLC can be subdivided further into squamous cell carcinoma and adenocarcinoma. [9] [24]

2.1.1 Diagnosis and staging of lung cancer

Diagnosis of lung cancer relies on the recognition of symptoms. The symptoms may be both vague and non-specific. Non-specific symptoms such as weight loss, anorexia, and fatigue often predominate in the symptomatic patient. The most common specific symptom is cough. Other specific symptoms may be e.g. breathlessness, chest pain, recurrent pneumonia, and haemoptysis. 15 % of patients are asymptomatic at the time a lung lesion suspected to be cancer is identified [9]. [9] [24]

The objectives of an examination of a patient with a lung lesion suspected to be cancer are generally to:

1. Make a diagnosis as efficiently as possible. If cancer is excluded an alternative diagnosis should be made.
2. Determine whether the cancer (if diagnosed) is primary (NSCLC or SCLC) or secondary.
3. Staging the cancer in order to plan a suitable treatment.

[9]

During the examination process different laboratory, radiographic, and invasive tests are conducted. The best method of obtaining a diagnosis depends on the location of the tumour. Laboratory tests may for instance include a full blood count where potential findings could be anaemia and pancytopenia. Radiographic tests may include a chest radiograph, where a potential finding could be a mass lesion, or a CT image of thorax, which could provide a definition of extent of the cancer. Invasive tests could be a bone marrow biopsy as bone marrow may be involved in SCLC. [24]

A suitable treatment of each individual case of lung cancer is determined by accurate staging. NSCLC is staged by applying the TNM system, where T stands for primary tumour, N stands for regional lymph nodes, and M stands for distant metastasis. In the TNM system, different tumour and metastasis descriptions are listed and the clinicians stage NSCLC based on these. In Table 2.1, stage grouping and prognosis for NSCLC, based on the TNM system, are seen. In the table, T1-T4 refer to different tumour descriptions, e.g. size and appearance of tumour, N0-N3 refer to different lymph node descriptions, e.g. type and position, and M1 refers to presence of distant metastasis, i.e. cancer has spread beyond the lungs. [9] [24]
In SCLC, a two-stage system is used instead of the TNM system, with the two stages being limited or extensive. In patients with SCLC staged as limited no evidence of metastasis disease is present and the disease is restricted to one side of the chest. In patients with SCLC staged as extensive, the patients have distant metastasis outside the ipsilateral hemithorax. [24]

Stage		TNM characteristics	Approx. 5-year survival
I	IA	T1N0	60-80 %
	IB	T2N0	
II	IIA	T1N1	50 %
	IIB	T2N1	
		T3N0	
III	IIIA	T1/2N3	10-25 %
		T3N1/2	
	IIIB	Any T, N3	
		T4, any N	
IV		Any T, any N, M1	<5 %

Table 2.1: The table shows stage grouping and prognosis for non-small cell lung cancer (NSCLC). T1-T4 refer to different tumour descriptions, e.g. size and appearance of tumour, N0-N3 refer to different lymph node descriptions, e.g. type and position, and M1 refers to presence of distant metastasis. [24]

2.2 Computed Tomography

As previously mentioned, CT images are often used in the diagnosis of lung cancer. To get a better understanding of how and why CT images are used in the diagnosis and treatment planning of lung cancer, the physics behind CT imaging is described.

2.2.1 History and principle of Computed Tomography

CT is a medical image technique employing tomographic imaging in which cross-sectional images of the body are created. CT imaging became possible in the 1960s as a result of the development of modern computer technology. Yet some of the ideas on which CT imaging is based can be traced back to the first half of the 20th century. In CT imaging, the images are created by means of x-radiation. X-radiation is a type of electromagnetic radiation and it is composed of x-rays. X-rays have energies in the range of 120 eV to 120 keV. X-rays in the range of 12 keV to 120 keV are characterized hard and are able to penetrate human tissue. Compared to radiography, in which body parts are imaged using x-radiation as well, x-radiation is applied at a more advanced level in CT imaging. [20] [10]

The principle of CT imaging consists of measuring the spatial distribution of a physical quantity to be examined from different directions and to compute images based on the acquired data. [20] The general process of data acquisition will be presented in Section 2.2.2, while the computation of images will be presented in Section 2.2.3. In these sections it is described how a single slice image is obtained. This is the process of sequential CT imaging which is one of two main categories of CT imaging. The other category being spiral CT imaging. Spiral CT imaging became available as further development of the applied technology was conducted. The principle of the two categories of CT imaging is generally the same, however the difference lies within the scanning time, which is reduced during spiral

CT. [20] As other medical image techniques, CT imaging is affected by artifacts influencing the quality of the images. This issue will be presented in Section 2.2.4.

2.2.2 Acquisition of data

In CT imaging, a narrow beam of x-rays is passed from an x-ray source through the patient and subsequently measured by an x-ray detector. The measured value at the detector is thus related to the total amount of matter placed along the path of the beam. Since the body consists of different types of matter with different characteristics, the beam of x-rays is attenuated differently, i.e. the different types of matter absorb x-rays in varying degrees. Bone and teeth for instance absorb more of the x-rays, resulting in a lower signal compared to soft tissue and fat. In Figure 2.2, a simple setup of a CT imaging system is illustrated in accordance to acquisition of data related to a single slice image, i.e. a cross-section of the body. [26] [20]

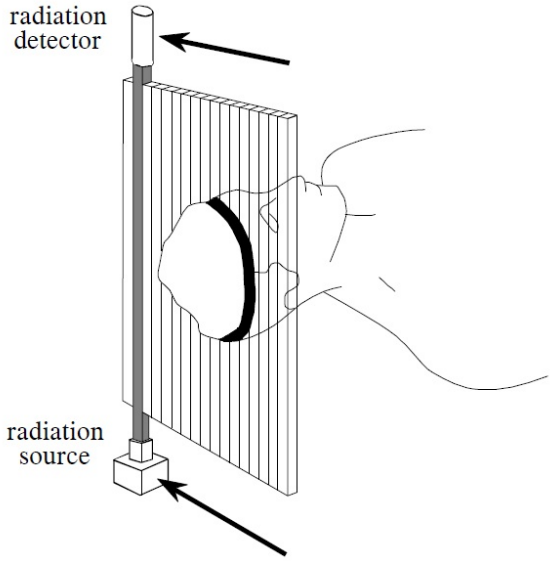

Figure 2.2: The figure illustrates acquisition of data related to a single slice image through the center of the head. [26]

As seen in the figure, a narrow beam of x-rays is passed through the head of the patient from source to detector. The source and detector assemblies are then translated to obtain a single *view* at that given angle. Data from additional views is however required to compute a CT slice image, and thereby visualize that particular cross-section of the body. The source and detector assemblies are thus subsequently to the translation, rotated in about 1° increments after which the translation process is repeated and the additionally views are acquired. In a CT imaging system, the x-ray source and detector are mounted on a rotating framework that surrounds the patient to enable the rotation process. [26]

Preprocessing of the measured data is necessary before a image reconstruction process can be conducted. The preprocessing e.g. involves taking the logarithm of each x-ray measurement. X-rays decrease in intensity exponentially as they pass through the body and by taking the logarithm, a signal which is linearly related to the characteristics of the matter being measured is provided. The preprocessing varies in regard to the applied type of x-rays

and detectors, and will not be mentioned further as they are not related to the image reconstruction process. [26] [20]

2.2.3 Image reconstruction

A number of different approaches to compute CT images given a measured set of views exist. These approaches are generally called CT reconstruction algorithms. Several approaches use algebraic iterative techniques during computation of CT images. The iterative techniques differ in the means by which the successive corrections are conducted. These are ray-by-ray, voxel-by-voxel, or simultaneously correcting the entire data set, respectively. As the iterative techniques are all relatively slow these are in general not applied in modern CT imaging systems. [26] [20]

Another type of reconstruction algorithm is filtered backprojection (or convolution-backprojection procedure). Filtered backprojection is based on the simple backprojection technique in which an image is reconstructed by taking each view and spreading it back along the path of the beam it was acquired. The computed image is a blurry version of the correct image. In filtered backprojection, each view is filtered before backprojection, hence to correct the blurring obtained in simple backprojection. The resulting image is an exact reconstruction of the correct image. In Figure 2.3, the principle of filtered backprojection is seen. Filtered backprojection is the most frequently applied reconstruction algorithm in modern CT imaging systems. [26] [20]

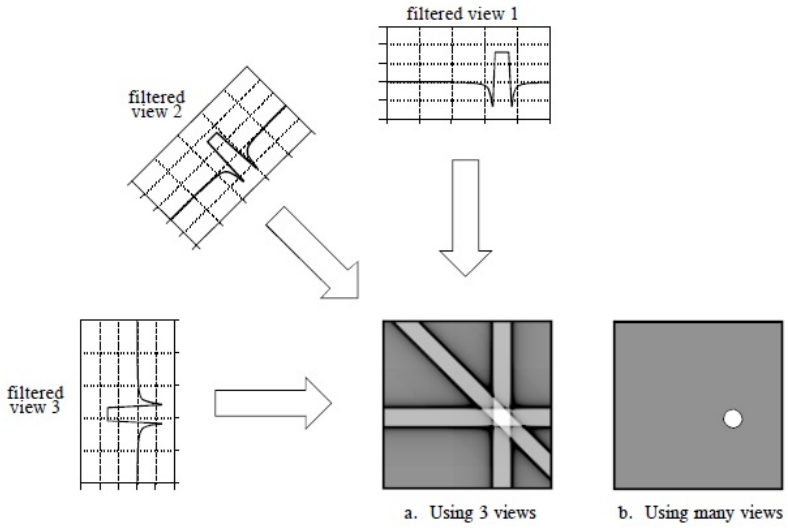

Figure 2.3: The figure shows the principle of filtered backprojection in which each view is filtered before backprojection. [26]

CT images are composed of minor volume blocks called voxels. Each voxel is represented by a set of coordinates in space, and each has a value, representing the grey-level intensity of that voxel in space. After reconstruction, each voxel in the CT images is normalized to obtain grey-level intensities between -1000 to +3000 measured in Hounsfield units (Hu). A grey-level intensity around -1000 Hu corresponds to air, soft tissues range from -300 Hu to

-100 Hu, water is 0 Hu, and dense bone and areas filled with contrast agent range up to +3000 Hu. [10]

2.2.4 Quality of CT images

CT imaging has the best contrast resolution when compared to other medical image techniques using x-rays. The contrast resolution depicts very subtle differences in contrast, since the noise is smaller than the difference between the grey-level intensities in the tumour and the surrounding tissue. Thus, CT imaging excels in distinguishing soft tissue tumours. The contrast resolution depends on the spatial resolution resulting in a trade-off between these two characteristics. [10]

CT imaging is as other medical image techniques affected by artifacts due to the physical nature of the image technique. Causes of artifacts in CT imaging are e.g. beam hardening and partial volume effects. As other medical image techniques, artifacts due to sampling errors and patient movement may occur as well. [20]
In CT images, beam hardening is primarily seen as dark zones or lines between bone structures, particularly during imaging in the area of the base of the skull. Beam hardening occurs when the beam of x-rays becomes more penetrating or harder as it passes through matter. [20] Partial volume effects occur when a voxel contains more than one type of tissue. The grey-level intensities of these voxels are instead a weighted average between the grey-level intensities of the corresponding tissues. [10]

2.3 Treatment of lung cancer

The type of treatment in regard to lung cancer depends on the progress of the cancer. A correct classification of the tumour and its possible spread is therefore as mentioned important to establish to ensure the most effective treatment. In general, cancer is mostly cured by surgery (49 %), followed by radiation therapy (40 %), and lastly by chemotherapy (11 %) [27]. Each type of treatment will be described in the following together with their respective side effects.

2.3.1 Surgery

Surgery offers the best chance of a cure in patients with NSCLC. But only approximately 30 % of patients with NSCLC are operable. For operable patients, the type of surgery depends on the location of the tumour and the respiratory capacity of the patient. Three different types of surgery exist, which are described in Table 2.2. [27]
Potential side effects vary in accordance to the type of surgery performed. Lobectomy and pneumonectomy can lead to the most severe side effects, as air and fluid may collect in the chest cavity. Patients who have undergone lobectomy or pneumonectomy often need assistance to restart breathing deeply. Common side effects due to surgery are furthermore pain, weakness in the chest and arms, and reduction in respiratory capacity. [27]

2.3.2 Chemotherapy

Chemotherapy is a drug used to destroy cancer cells. Chemotherapy interferes with the cell cycle, which can be divided into different steps by certain checkpoints, which are regulated by:

Name	Procedure	Indication
Wedge/segmental resection	Removal of a small portion of the lung along with healthy tissue that surrounds the tumour.	If the tumour is peripheral with no evidence of local extensions.
Lobectomy	Removal of one entire lobe in the lung. The most common type of surgery for lung cancer.	Centrally located tumours contained within a single lobe.
Pneumonectomy	Removal of one entire lung.	Tumours originating within the main stem bronchus, where the primary tumour involves more than one lobe, or where the hilum is involved.

Table 2.2: The table shows the three different types of surgery for non-small cell lung cancer.

1. Cyclin-dependent kinases (CDK) which phosphorylate cyclins (regulatory proteins).
2. Cyclins.
3. Cyclin-dependent kinase inhibitors (CDKL), which are negative regulators of the CDK-cyklin complex.

Some kinds of chemotherapy act at specific points in the cell cycle whereas others are not specific to any point. [24]
Chemotherapy is most often used in combination with either surgery or radiation therapy. For advanced lung cancer it is the preferred choice of palliative treatment. Chemotherapy can be used both prior to or after surgery. Studies have shown that some patients with lung cancer can greatly benefit from receiving chemotherapy prior to surgery to manage micrometastases or even reduce the size of the primary tumour. Numerous studies have shown, adjuvant chemotherapy after surgery increases the chance of survival. [9]

Chemotherapy interferes with the synthesis or function of DNA and is more toxic to proliferating cells. The toxicity occurs at sites with rapid cell turnover, such as the gastrointestinal mucosa, hair follicles, and the bone marrow. Toxicity can be divided into:

- Immediate - nausea, vomiting, loss of hair, infection risk.
- Late - secondary malignancies, infertility, cardiac, pulmonary or renal impairment.

[24]

2.3.3 Radiation therapy

Radiation therapy is the most common type of treatment for NSCLC. More than 50 % of patients receive this treatment at some point during their illness. Radiation therapy features accurate delivery of high-energy photon (x-ray) beams targeted at the cancer. The beams

are produced using electricity by a purpose-built machine, named a linear accelerator. [9] The beams produce free radicals within the cell which interact with the DNA causing various types of damage. If a sufficient amount of damage is done to the cell it is unable to repair itself, causing the cell to die or lose its ability to replicate. [24] Figure 2.4 shows an illustration of a typical linear accelerator used in radiation therapy.

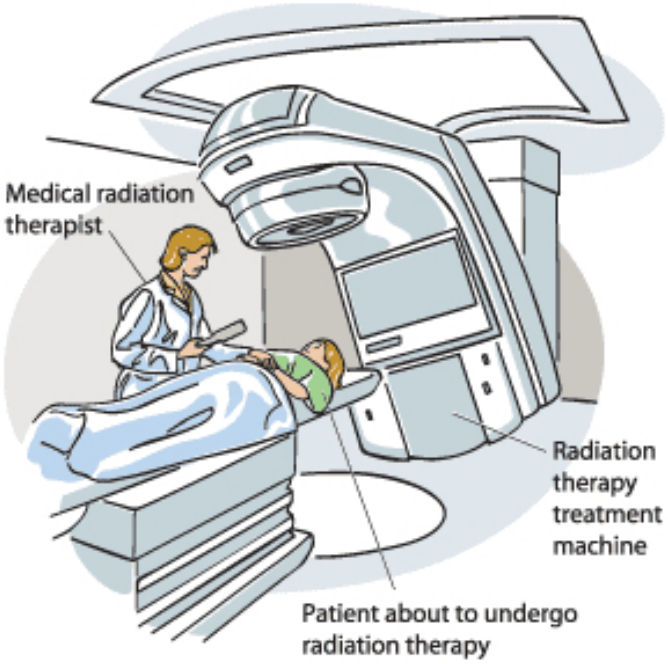

Figure 2.4: The figure shows a typical linear accelerator used in radiation therapy. [2]

The probability of cure, named tumour control probability (TCP), and the incidence of side effects depend on a number of factors, namely the total dose delivered, the dose delivered per fraction, and the overall treatment time. Radiation therapy is conventionally delivered in daily fractions for four to six weeks. By decreasing the overall treatment time the TCP is increased, but if the decrease in overall treatment time is achieved by increasing the dose per fraction the risk of late radiation side effects is increased. Instead, research into hyperfractionation, i.e. more than one treatment per day, has been made. Using hyperfractionation results in constant risk of late radiation side effects and significantly decreases the overall treatment time. However, there must be at least six hours between each fraction to allow for normal tissue to repair. [9]

Radiation therapy can be either radical with intention of cure or palliative. Palliative radiation therapy has the aim to maximise the symptomatic benefit with the least side effects in the quickest possible time. Radical radiation therapy concerns two groups of patients: inoperable patients and patients who are operable but also have respiratory or cardiovascular diseases. In the planning of radiation therapy the visible cancer is outlined on the computerised planning system based on imaging studies and other clinical tests. The outlined cancer is known as the gross tumour volume (GTV). The GTV is grown by applying a three-dimensional computer algorithm in all directions to account for microscopic spread, patient movement during treatment, and organ motion during breathing. The volume re-

sulting from this procedure is known as the planning target volume (PTV). Each patient gets an individualised treatment plan, which optimises the radiation therapy delivery to the cancer while minimising the dose to the critical normal tissues of the lungs and spinal cord. The treatment is usually delivered via a number of radiation beams which are shaped in the machine head by multileaf collimators. This reduces the volume of normal tissue irradiated, minimising side effects and damage. A conventional treatment of radiation therapy consists of a total dose of 66 Gy at 2 Gy per fraction over 6.5 weeks keeping the dose to normal tissues within safe limits [24]. [9]

Within the first month of radiation therapy little symptomatic reaction is noticeable. Irritation of the larger bronchioles and bronchi with cough may occur during radiation therapy. After 1 to 3 months after completion of radiation therapy, clinical pulmonary reactions are expressed as a pneumonitic process. An example of pneumonitis is seen in Figure 2.5.

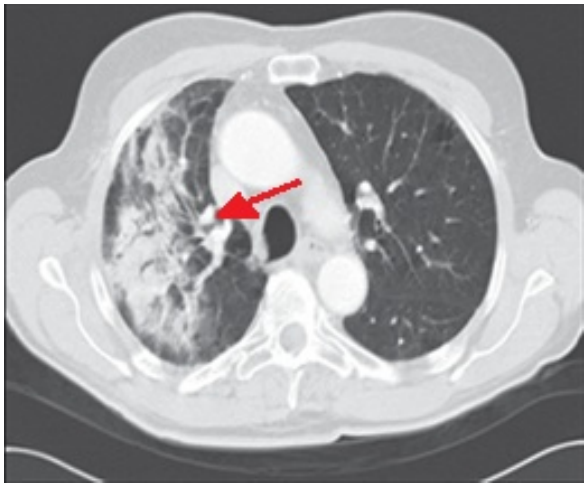

Figure 2.5: The figure shows an example of pneumonitis, which is indicated with the red arrow. [5]

The severity of the symptoms due to acute pneumonitis depends on the degree of pulmonary involvement. Symptoms which may arise are low-grade fever, nonspecific respiratory symptoms such as congestion, cough, and fullness in the chest. Dyspnea, pleuritic chest pain, and nonproductive cough may arise in more severe cases. The pneumonitic phase with the acute symptoms is generally relatively short in duration. After the acute phase an intermediate phase occurs where the histologic changes continue but where the symptoms are not as pronounced. The intermediate phase progresses into the eventual fibrotic state. Most patients with radiation fibrosis are asymptomatic. [15]

Radiation pneumonitis has an incidence of 1 % to 20 %. Radiation fibrosis occurs 6 to 24 months after completion of radiation therapy and usually remains stable after 2 years. The radiological changes due to radiation pneumonitis are confined to the field of irradiation. In the irradiated region there is, initially, a diffuse haze with obscuring of vascular outlines. Irregular consolidations appear which fuse to form a sharp edge corresponding to the field of irradiation. These appearances may gradually clear and dissapear but they may also lead to fibrous changes resulting in radiation fibrosis. [13]

To grade the degree of side effects different scoring systems exist. An example of one of these systems, from the Radiation Therapy Oncology Group, is shown in Table 2.3. [19]

Grade	**Acute**	**Late**
1	Mild symptoms of dry cough or dyspnea on exertion.	Asymptomatic or mild symptoms (dry cough), slight radiographic appearances.
2	Persistent cough requiring narcotic, antitussive agents, dyspnea with minimal effort but not at rest.	Moderate symptomatic fibrosis or pneumonitis (severe cough), low grade fever, patchy radiographic appearances.
3	Severe cough unresponsive to narcotic antitussive agent or dyspnea at rest, clinical or radiologic evidence of acute pneumonitis, intermittent oxygen or steroids may be required.	Severe symptomatic fibrosis or pneumonitis, dense radiographic changes.
4	Severe respiratory insufficiency, continuous oxygen or assisted ventilation.	Severe respiratory insufficiency, continuous oxygen, assisted ventilation.
5	Death	Death

Table 2.3: The table shows one scoring system, from the Radiation Therapy Oncology Group, which enables grading of side effects after radiation therapy. [19]

Although different scoring system exist, they do not provide an accurate assessment of the side effects. They do not entail enough detail and at some grades they are not consistent with each other, making the diagnosis difficult and not very quantitative. [6]

Chapter 3

Problem statement

In this chapter, the themes and issues presented in Chapter 1 and Chapter 2 are shortly summarized, and then followed by a presentation of the aim of this project.

3.1 Summary

Lung cancer is the leading cause of cancer related deaths in the world and non-small cell lung cancer (NSCLC) is the most common type. Lung cancer is diagnosed based on symptoms, laboratory tests, and radiographic tests. Computed Tomography (CT) is often used in the diagnosis of lung cancer since this image technique excels in distinguishing soft tissue tumours. CT images are also used in the treatment planning. Even though surgery offers the best cure of lung cancer more than 50 % of the patients receive radiation therapy at some point during their treatment. Some tumours are inoperable and some patients also have respiratory or cardiovascular diseases making them unqualified for surgery. Radiation therapy uses x-ray beams targeted at the cancer. The x-ray beams cause damage to the cancer cells causing the cells to die or lose their ability to replicate. To compensate for patient movement, organ motion, and microscopic spread a larger area than the tumour is irradiated during radiation therapy. This may cause side effects and damage to the normal tissue of the lungs. Acute pneumonitis occurs in 1 % to 20 % of NSCLC patients three months after completion of radiation therapy. The radiological changes due to pneumonitis are confined to the field of irradiation. In the CT images irregular consolidations of diffuse hazes will appear when pneumonitis is present. These changes may disappear but may also lead to fibrous changes resulting in radiation fibrosis. To grade the side effects of radiation therapy different scoring systems exist. The scoring systems do not provide an accurate assessment of the side effects since they do not entail enough detail and they are not consistent, making the diagnosis difficult and not very quantitative.

3.2 Aim of the project

Based on the themes and issues presented in Chapter 2 and the above mentioned, the aim of this project is to:

Develop a method which enables quantification of lung damage after NSCLC treatment with radiation therapy, using baseline and three month follow-up CT images.

In the remainder of the report, the term lung damage covers pneumonitis. The baseline CT images were acquired just prior to radiation therapy.

Delimitation of the project
If a patient does not develop lung damage, a difference between baseline and follow-up CT images should be present since the result of radiation therapy should be a shrunken or even disappeared tumour. In patients who have developed lung damage, a difference may not be present since some of or the entire tumour has been replaced by lung damage.

Given the presented aim of this project, the scopes of this project are narrowed down to:

- Determine whether a difference between baseline and follow-up CT images is present.
- Examine whether this difference can be quantified in such way that it can be determined that a patient has developed lung damage.

Chapter 4

Presentation of methods for image analysis

In this chapter, segmentation and texture analysis of medical images will be presented. These are both types of image analysis which are commonly applied in problem areas such as the one in this project. In Section 4.1, segmentation of medical images is introduced and common applied methods of segmentation are described. In Section 4.2, texture analysis of medical images is introduced after which common applied methods are described. The aim of this chapter is to present possible directions of this project in regard to which methods could be applied and for what reason.

4.1 Segmentation of medical images

Medical images, e.g. Computed Tomography (CT) images, are assisting greatly in clinical diagnosis and the following treatment. Medical images provide multi-orientation views and details of organs and structures, and generally with high resolution as well. Segmentation of such medical images becomes relevant in quantitative studies centered around specific organs, structures, or comparisons between them. Segmentation generally refers to a partition of an image into regions. [18] Several segmentation methods exist, e.g. pure manual segmentation methods and computer-aided segmentation methods. In manual segmentation methods, contours of a region is sketched slice by slice using pointing devices and such methods are thus very time-consuming and user-dependent. Computer-aided segmentation methods use algorithms that make the segmentation far less time-consuming and enhance the accuracy. In segmentation of medical images, the employed segmentation method should reflect the image technique involved since appearances of the same organs or structures often differ between the image techniques. *A priori* knowledge such as the biomechanical behaviour of organs and structures are often taken into account as well. [17]

Segmentation methods can be divided into three main types based on their principal techniques. These are those based on thresholds, those based on clustering techniques, and those based on deformable models, respectively. It is common however, that a given segmentation method uses multiple segmentation techniques. Hence, for some segmentation methods a definite categorization can not be made. [17] The three main types of segmentation methods are described in the following sections, with focus on CT images.

4.1.1 Threshold-based segmentation methods

Threshold-based segmentation methods are employed when relevant organs or structures have distinctive features such as image intensity or gradient magnitude. Hence, the segmentation process relies on these features. In the segmentation process, a search for voxels having values within ranges defined by thresholds is conducted. The thresholds can be selected both manually or automatically. In a manual selection of thresholds, *a priori* knowledge is necessary, while in an automatic selection of thresholds, they can be defined by e.g. using an image histogram which graphically represents the distribution of grey-level intensities in an image. [8] Segmentation methods of this type can be further categorized as edge-based, region-based, or hybrid. This categorization is based on how the thresholds are defined. [17]

In edge-based methods, thresholds are related to the edge information since organs and structures can be represented by edge points. The aim of the applied algorithms is to find edge voxels and eliminate potential noise influence. Edge voxels can be found as there is often a sharp change in grey-level intensity at edges between different organs and structures. An example of an edge-based method is the Laplacian edge detection. It uses the second derivation information of the image grey-level intensity to find edge voxels. It is often necessary to apply postprocessing techniques like morphological operations to connect breaks in the detected edges. [17] [18]
In region-based methods, the applied algorithms aim to search for voxels with similar feature values and coherent regions are found directly. The rules defining the search vary among the different methods. A simple approach can be to select an initial seed point which is then expanded subsequently by appending neighbouring voxels if their grey-level intensities lie within prior selected thresholds. This is an example of seeded region growing, one of several region-based methods. Region-based methods may have difficulties controlling any leakage from the region due to the dependency on grey-level intensity. [17] [18]
In hybrid methods, the applied algorithms embody many of the concepts of the two other types of methods. Segmentation based on watersheds is an example of this type of method. The concept of watersheds is to consider images as reliefs and treating the gradient magnitude as elevation. The aim of the applied algorithm is to find watershed lines during successive flooding of the relief. A watershed line consists of voxels with local maximum gradient magnitudes. Image regions are defined as the voxels enclosed by the same watershed line. Over-segmentation may occur when hybrid methods are employed, especially if the image is noisy. [17] [18]

4.1.2 Clustering-based segmentation methods

Segmentation methods of this type exploit the fact that medical images can be treated as patterns. Segmentation can thus be conducted using patten recognition techniques. The two main types of clustering-based segmentation methods are those applying supervised classification techniques and unsupervised classification techniques, respectively. [17]

Supervised classification techniques include among others k-nearest neighbour classifiers and supervised artificial neural networks (ANN). Training data is needed to extract structure information when these techniques are applied. How the training data is used varies however. A k-nearest neighbour classifier has a training phase in which feature vectors and class labels of the training samples are stored. In the training phase, k nearest stored points are selected

for each unlabeled point according to a point distance. An unlabeled point is then classified by e.g. finding the most frequent class label appearing within the selected points. [17] [3]
Supervised ANNs can be used to model complex relationships between input and output. They function as non-linear statistical data modeling tools in which weights in different layers are updated after processing each sample to minimize a cost function. The cost function is defined by the features of the structures. Information extracted from training data provides the features in form of weights used for the segmentation. ANNs are commonly used for segmentation of images inside which the organs and structures of interest have relatively stable shapes. [17] [3]
Unsupervised classification techniques include among others fuzzy C-means algorithms and unsupervised neural networks. No training data is needed as features are extracted from the classified points. Fuzzy C-means algorithms are fuzzy clustering techniques which provide soft segmentations by calculating the probability that a voxel belongs to a given cluster, i.e. a given group of voxels. Hence, an unlabeled voxel is assigned to different clusters with varying membership, determined by the calculated probability. Soft segmentations are often preferred when working with medical images as these are influenced by partial volume effects which cause image blurring. Hence, a single voxel may represent more than one organ or structure. In unsupervised neural networks, the weights of the neural network are trained according to a learning rule. The learning rule could for instance be a *winner-takes-all* rule in which a single weight is assigned the value of 1, while the others are assigned the value of 0. [17] [3]

4.1.3 Deformable model-based segmentation methods

Deformable model-based segmentation methods are far more flexible than threshold-based and clustering-based segmentation methods. Segmentation methods of this type are thus often used for rather complex segmentations. They treat organ and structure boundaries as the final status of initial contours, and the segmentation process can generally be described as a modeling of contour evolution. The segmentation methods of this type use either parametric deformable models or geometric deformable models. These mainly differ in how tracking of the moving contour is conducted. [17]

A parametric deformable model tracks contour evolution using sampled contour points. The initial contour is represented by a moving equation which is derived through energy functions or defined directly by dynamic forces. Energy functions generally include the internal energy and the external energy. The aim of the internal energy is to maintain the regularity of the contour, and it can be defined by geometric properties of the contour, e.g. length and area. The aim of the external energy is to attract the contour to the boundary, and the image information is used to define the external energy. *A priori* knowledge is often incorporated when defining energy functions, initial conditions etc. Algorithms applied using parametric deformable models mainly differ in their definitions of external forces. Parametric deformable models may have difficulties with handling topological changes, i.e. it is sometimes necessary that the initial contour has the same topology as the desired boundary. Also, the initial contour should be placed near the desired boundary to ensure external forces that are strong enough. [17]
Geometric deformable models can easily handle topological changes, and are able to calculate the geometric properties of the contour implicitly. This is done by applying the level set method. [17]

4.2 Texture analysis of medical images

Texture analysis is a common used technique in regard to analysis and interpretation of medical images. The texture of images refers to the appearance, structure, and arrangement of regions within the image. Texture analysis is generally used to classify regions of interest in images, e.g. with the purpose of differentiating between healthy and pathological tissue. Texture analysis can also be used for segmentation of medical images. In texture analysis, an amount of texture features is determined, and based on these it should be possible to decide whether they provide the differentiation required. Hence, texture analysis enables region description, and it is a useful way of increasing the information obtainable from medical images. Texture analysis has mainly been conducted in 2D images, i.e. slices of 3D medical images have been processed individually. [8] [16] In the following, different methods for texture analysis will be described. The descriptions will be restricted to pixels.

Methods for texture analysis of medical images can be categorized as either structural, model-based, statistical, or transform methods. With structural methods, texture is described by using primitives, i.e. a square object is represented by straight lines or other primitives that are able to form its boundary. The advantage of structural methods are their high symbolic description of the image, but they lack content in regard to deeper analysis of texture. In model-based methods, the aim is to describe texture by applying mathematical models, e.g. different stochastic models, and base the analysis on estimated texture features. The computational complexity of texture feature estimation is often high and thus a disadvantage. Statistical methods obtain knowledge about the distribution and relationship of grey-level intensities in the image, and the texture analysis is conducted applying that knowledge. Statistical methods are the most common applied methods in texture analysis of medical images. With transform methods, texture analysis is conducted in a different space, e.g. the frequency space. Transform methods are based on either the Fourier, Gabor, or Wavelet transform. The Wavelet transform is applied often as it can easily be adjusted to a given problem. The majority of the most commonly used texture features are derived from statistical methods such as image histogram, absolute gradient, run-length matrix, and co-occurrence matrix. These methods will be described in the following. [8]

4.2.1 Image histogram

As mentioned in Section 4.1.1, an image histogram provides a graphical representation of the distribution of grey-level intensities in an image. Hence, the number of pixels for each grey-level intensity is counted. From an image histogram several texture features can be derived. These texture features may be its mean, variance, and standard deviation which are all listed in Table 4.1. The mean provides the mean grey-level intensity in the image, while the variance provides a measure of how far from the mean the grey-level intensities are distributed. Finally, the standard deviation provides a measure of the variability in grey-level intensities. [8] [18]

A texture analysis based on texture features derived using only image histograms provides no information in regard to the relative position of pixels with respect to each other. It is the simplest method of all in the field of texture analysis. [8] [18]

Feature	Formula
Mean (μ)	$\frac{1}{n}\sum_{i=1}^{n} X_i$
Variance (σ^2)	$\frac{\sum(X_i-\mu)^2}{n}$
Standard deviation (σ)	$\sqrt{\sigma^2}$

Table 4.1: The table shows texture features which can be derived from an image histogram and the formula by which they are expressed.

4.2.2 Absolute gradient

An absolute image gradient reveals the spatial variation of grey-level intensities across the image. An abrupt variation in grey-level intensities at a given point in the image will be represented by a high absolute gradient value, while the opposite will be represented by a low absolute gradient value. The order of variation (dark to light or light to dark) is not taken into account, hence *absolute*. A gradient image will emphasize the contours in an original image, and the contours will be most clear at points where the grey-level variation is most evident. Texture features which may be derived from the absolute gradient include its mean and its variance, as it was the case with the image histogram. The mean of the absolute gradient provides the mean grey-level variation across the image, while its variance provides a measure of how far from the mean the variations are. [8]

4.2.3 Run-length matrix

The computation of a run-length matrix involves a search in an image for runs of pixels having the same grey-level intensity. The search is conducted across a defined direction, i.e. e.g. in the horizontal or vertical direction. Given a direction, the number of times there are runs of pixels having the same intensity is counted. This is conducted for each allowed grey-level intensity and with different run sizes. Each entry of the matrix is filled with the number of runs which have been counted. The size of the matrix is thus determined by the number of grey-level intensities and run sizes. Different matrices can be computed as the direction can be changed. Texture features which may be derived include the fraction of image in runs and the short-run emphasis. The fraction of image gives the percentage of pixels that are part of any of the runs included in computation of the matrix. The short-run emphasis measures the proportion of runs occurring in the image that have short length. [8]

4.2.4 Co-occurrence matrix

A co-occurrence matrix is computed by searching an image for pairs of pixels that possess a given distribution of grey-level intensities. Initially, a displacement vector with a direction and a distance is defined, and pairs of pixels separated by this displacement vector across the image are evaluated. A count of the number of pairs of pixels that possess a given grey-level distribution is conducted and the numbers are filled into the matrix. The matrix is a n x n matrix, where n is the range of grey-level intensities in the image. Hence, each entry of the matrix corresponds to a possible distribution of grey-level intensities in the image. Co-occurrence matrices are computed for different displacement vectors in regard to a single

image. [8]

In Figure 4.1, an example of how a co-occurrence matrix is computed is illustrated. In the figure, an image is seen to the left with grey-level intensities ranging from 1 to 8. The size of a corresponding co-occurrence matrix, which is seen to the right, is thus 8 x 8. The computation is conducted in the horizontal direction where it is always the neighbour pixel to the right which is evaluated. Entry (1,1) of the co-occurrence matrix is filled with 1 as only one pair of neighbouring pixels in the image is having grey-level intensity 1, in the given direction. In return, entry (2,6) of the co-occurrence matrix is filled with 3 as three pairs of neighbouring pixels in the image have grey-level intensities 2 and 6 respectively, in the given direction. [18]

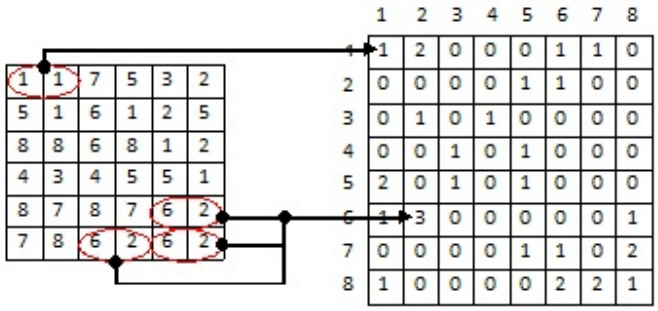

Figure 4.1: The figure shows how a co-occurrence matrix is computed. To the left an image with grey-level intensities ranging from 1 to 8 is seen, and to the right the corresponding co-occurrence matrix is seen. The computation is conducted in the horizontal direction and it is the neighbour pixel to the right which is evaluated. Adapted from [18].

The choice regarding the direction and distance of the displacement vector varies for different applications. Studies often use different directions and distances, resulting in many matrices and thus texture features making the computation very comprehensive. To evaluate the texture features in these studies, an average of each texture feature from all the matrices is derived. [4] [8]

Texture features which may be derived from a co-occurrence matrix include contrast and correlation. The contrast refers to the difference in grey-level intensities between pairs of pixels over the entire image. The correlation measures the joint probability occurrence of the pairs of pixels that are represented. Other texture features which can be derived include energy and homogeneity. The energy provides the sum of squared elements in the co-occurrence matrix, while the homogeneity measures the closeness of the distribution of entries in the co-occurrence matrix to the diagonal of the matrix. The mentioned texture features are listed in Table 4.2. To be able to derive texture features from a co-occurrence matrix, the matrix have to be symmetrical and the entries normalized. [8] [18]

4.2.5 Texture analysis of volumetric data

As described in Section 2.2, a CT image is composed of voxels which all have a grey-level intensity, i.e the CT images are volumetric images. Texture analysis has, as mentioned, mainly been conducted in two-dimensional (2D) images and slices of three-dimensional (3D)

Feature	**Formula**	**Value range description**
Contrast	$\sum_i \sum_j \lvert i-j \rvert^2 P(i,j)$	Range is $\left[0;(n-1)^2\right]$, where the contrast is 0 for a constant image.
Correlation	$\sum_i \sum_j \frac{(i-\mu)(j-\mu)P(i,j)}{\sigma^2}$	Range is $[-1;1]$, where the correlation is 1 or -1 for a perfectly positively or negatively correlated image.
Energy	$\sum_i \sum_j P(i,j)^2$	Range is $[0;1]$, where the energy is 1 for a constant image.
Homogeneity	$\sum_i \sum_j \frac{P(i,j)}{1+\lvert i-j \rvert}$	Range is $[0;1]$, where the homogeneity is 1 for a diagonal matrix.

Table 4.2: The table shows texture features which can be derived from a co-occurrence matrix and the formula by which they can be expressed. Additionally, the table contains a description of which values the texture features can have.

medical images have thus been processed individually. Such a texture analysis suffers from the drawback that important information is ignored. [16] Extending the methods described above to voxels and volumetric images is often straightforward. The co-occurrence matrix described in Section 4.2.4 is the traditional 2D co-occurrence matrix for 2D images. A 3D co-occurrence matrix exists as well, and the main difference is that it is computed by summing pixel triplet occurrences, instead of pixel pair occurrences. Computation of a 3D co-occurrence matrix can easily become very comprehensive, and deriving texture features from a whole 3D co-occurrence matrix will be time consuming. Kurani et al. published a paper in which an approach for computation of a co-occurrence matrix for volumetric images is presented [4]. In this approach, the texture analysis is still in a 2D co-occurrence matrix form, but it is able to capture the spatial dependence of grey-level intensities in volumetric images. This is conducted by summing the occurrences of pairs of voxels within the CT images. The approach showed promising results and is computationally efficient. [8] [4]

Chapter 5

Method for quantification of lung damage

In this chapter, the applied methods to fulfil the aim of this project, cf. Chapter 3, are presented. An overview of the main phases involved in fulfilling the aim of this project is given in Figure 5.1.

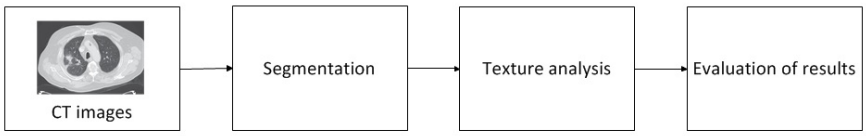

Figure 5.1: The figure shows the main phases involved in quantifying lung damage. The CT image is adapted from [5].

As can be seen in Figure 5.1, a segmentation of the Computed Tomography (CT) images is conducted to obtain only the lungs. The segmentation of the lungs enables a texture analysis of lung tissue, which thus is the next phase. The texture analysis involves extraction of image histogram-data and computation of a co-occurrence matrix for volumetric data. During the texture analysis, a number of texture features are derived. Based on the texture features, an evaluation of the results will be conducted. The choice of methods will be stated in the corresponding sections in which the phases are described.

In this chapter, the available data will be presented initially to determine what further processing needs to be done. MINC, which is the software tool used for the image processing, will be described as well. Subsequently the individual phases will be described.

5.1 Description of data

The data consists of CT images of thorax and the upper abdomen. The CT images have been conducted in Denmark between 2007 and 2010. Data from patients, who have undergone treatment for non-small cell lung cancer with radiation therapy, is available. All patients were given radiation therapy due to an inoperable lung tumour. For each patient a set of

CT images is available. Each set consists of a 3D baseline CT image, which was conducted prior to radiation therapy, and a 3D follow-up CT image, which was conducted three months after completion of radiation therapy.

The CT images were conducted using CT scanners from Siemens AG, GE Healthcare A/S, and Philips. The slice-thickness ranges between 2 mm and 5 mm.

Lung damage has been diagnosed in some of the patients following treatment with radiation therapy. This diagnosis has been established by a radiologist and a medical student. Some patients were excluded from the project, due to collapse of the lung or an insufficient segmentation of the lungs, cf. Section 5.3. Hence, in this project 8 patients with lung damage and 14 patients without lung damage are included. It is known for all subjects in which lung the tumour is located.

5.2 Tools for visualisation and interaction with data

The McConnell Brain Imaging Centre of the Montreal Neurological Institute, McGill University, Canada, has developed and released a package containing the MINC file format, toolbox and associated tools. [1]

MINC has two tools available to visualise and interact with MINC files. These are Register and Display, respectively. Register can be used to superimpose two volumes and to perform manual registration. Display can be used to manipulate and display 3D volumes like the available CT images. Both of these tools have been used during this project for different types of image processing.

The MINC file format and toolbox are platform independent and were originally written and released by Peter Neelin in 1992. Associated tools for e.g. image visualisation and registration were written and released afterwards. A library named the BIC Volume IO Library was developed by David MacDonald in 1995, and it is designed to link MINC files with C source code. It contains a set of functions for reading, writing, and manipulating volumes of medical imaging data. [23] [1]

5.3 Segmentation of CT images

To be able to conduct texture analysis of lung tissue, preprocessing of the CT images is necessary. The CT images are acquired with scanners from three different manufacturers, causing the spatial resolution in some instances to differ between the baseline CT image and the follow-up CT image. A large difference between the volume of the lungs may also be present between the baseline CT image and the follow-up CT image due to the different manufacturers. An initial registration of the baseline CT image and the follow-up CT image is thus conducted. Ideally, a one-to-one mapping between voxels in the two images would be preferable, making the texture analysis more local. Different automatic linear transformations have been applied with the aid of mutual information, but an overall acceptable result has not been possible. Instead, a manual registration has been conducted with the tool Register, mentioned in Section 5.2. In this registration, tags are manually placed in each baseline and follow-up CT image. The tags are placed in the contour of the lungs at

approximately the same height in both images. An affine transformation, consisting of three rotations, three translations, three scales, and three shears, was applied to the follow-up CT image to make the mapping between the tags. The registration is not perfect but it ensures that the volume of the lungs are approximately identical. In the preprocessing, the follow-up CT image is also resampled by trilinear interpolation to obtain the same size of the voxels as in the baseline CT image. Resampling is commonly used in image processing when it is desired to resize (shrink or zoom) an image, and it is basically interpolation that is conducted. Trilinear interpolation uses the eight nearest neighbors to estimate a new position of a point in space. [18] In Figure 5.2, a screenshot from Register is shown, with a baseline CT image (left), follow-up CT image (middle), and the two images (right) superimposed with the registration based on the tags (indicated with rings in the images).

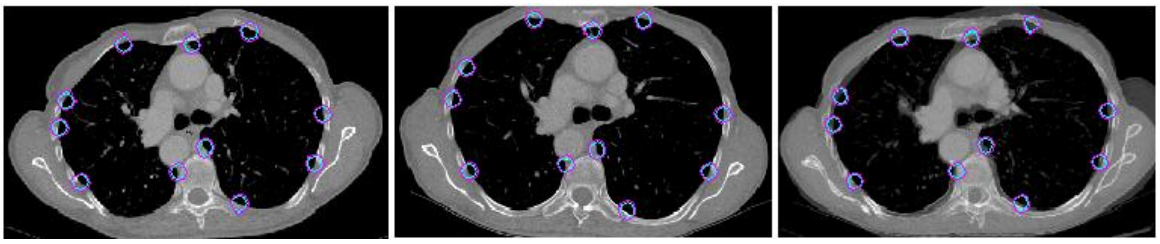

Figure 5.2: The figure shows a screenshot from Register with a baseline CT image (left), follow-up CT image (middle), and the two images superimposed (right).

Subsequent to the initial registration, the lungs are segmented to enable texture analysis. The lungs are essentially elastic bags of air in the body. In CT images, they are seen as dark regions and the contrast between the lungs and the surrounding tissues is clearly visible. Since there is a large contrast between the lungs and their surrounding tissues the type of segmentation chosen is seeded region growing which was described in Section 4.1.1. The tool Display, which was mentioned in Section 5.2, offers the possibility to make a seeded region growing by specifying the range of intensities contained in the lungs. A connectivity of 8 is chosen, meaning that the algorithm performing the region growing uses 8 neighbours during the growing process, until none of the neighbours are within the specified range of intensities. The seed points are manually chosen. After region growing, morphological operations are applied to close the gaps within the lungs. Initially two dilations are made to close the gaps. The dilations cause the contours of the segmentation also to dilate. This is reversed by applying two erosions. The segmented image consists of 1s within the lungs and 0s in the rest of the image. The final segmentation is verified by opening the original image with the segmented image on top. In Figure 5.3, a CT image is shown with the matching segmented image marked with red.

Following the segmentation and prior to the texture analysis, the segmented CT image is manually divided into the left and right lung, respectively. The division is conducted to enable a texture analysis of each lung individually. Since the lungs differ in shape, in some instances it is difficult to make a clear division between the two lungs. An example of such a division is seen in Figure 5.4, where the division between the two lungs is not perfectly clear. The division is made with best ability and with a minimum of error.

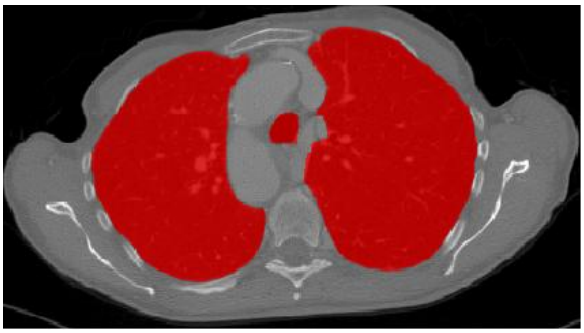

Figure 5.3: The figure shows a screenshot from Display with a CT image and the matching segmented image marked with red.

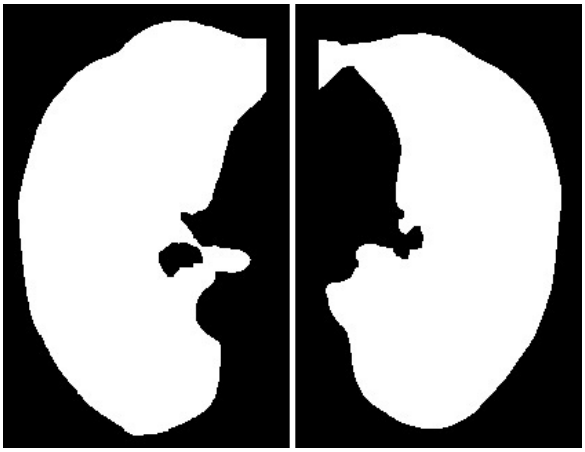

Figure 5.4: The figure shows a segmented CT image which has been divided into the left and right lung, respectively. As can be seen in the figure, the division between the two lungs is not perfectly clear.

It has been noticed that in few instances a leakage to surrounding tissue occurs. Some patients were excluded from this project due to too much leakage. In other instances, the leakage is assessed to be acceptable. Figure 5.5 shows two CT images of these instances from the front. On the left, a CT image of a patient who was excluded due to the extent of the leakage is seen. In the CT image, it is not evident how the leakage extend toward the posterior. On the right, a CT image of a patient who was not excluded is seen. The leakage in this CT image does not extend much outside the front view.

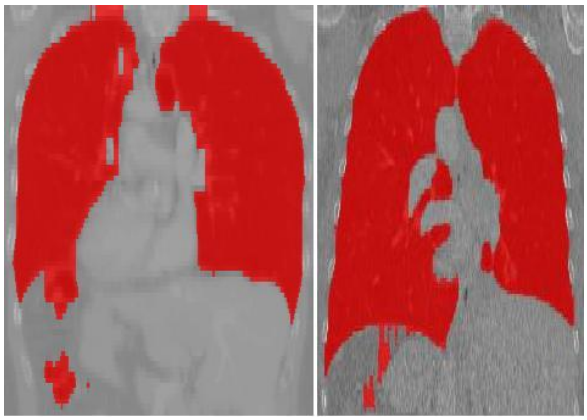

Figure 5.5: The figure shows two CT images of which the left was excluded from this project and the right was assessed to be suitable.

5.4 Texture analysis of CT images

Once the lungs have been segmented, a texture analysis to derive texture features is conducted. The texture features are used to characterise the tissue of the lungs, and the aim is to examine whether the texture features enable a differentiation between patients without lung damage and patients with lung damage, cf. Chapter 3. In this project, texture features from image histogram-data and a co-occurrence matrix are derived. Both of these methods, which were described in Section 4.2, have been used in quantitative studies in which e.g. a differentiation between healthy and pathological tissue is desired [8]. From the image histogram-data, mean, variance, and standard deviation are derived as these are commonly derived texture features from this texture analysis method [8]. In 1973, Haralick et al. published a paper in which texture features which can be derived from a co-occurrence matrix are listed and described [14]. Numerous quantitative studies computing co-occurrence matrices, e.g. [4] and [11], derive texture features as described by Haralick, although a varying amount of the Haralick texture features are derived. In this project, contrast, correlation, energy, and homogeneity are the Haralick texture features which are derived from the co-occurrence matrix. In Section 4.2.5, an approach for computation of a co-occurrence matrix for volumetric images was mentioned. As this approach showed promising results, the principle of this approach has been applied in this project for computation of a co-occurrence matrix [4]. In Section 5.5 and Section 5.6, the extraction of image histogram-data and the computation of a co-occurrence matrix, in this project, is described. In each section it is additionally described how the texture features are derived. Texture analysis is conducted on each lung in each CT image. Hence, 88 texture analyses are conducted in this project.

5.5 Image histogram

To obtain image histogram-data, an extraction of grey-level intensities from the lung in the CT image is conducted. Prior to the extraction of grey-level intensities, the segmented CT image and the corresponding original CT image are resampled to common voxel size. To extract grey-level intensities in the CT images the following steps must be carried out:

- A segmented CT image and the corresponding original CT image should be taken as inputs.
- Each voxel with a value above 0 in the segmented CT image should be identified.
- The corresponding voxels in the original CT image should be identified.
- The grey-level intensities in each of these voxels should be extracted and written to a text file.

This functionality is implemented in C as it is able to handle large amounts of data efficiently. As mentioned in Section 5.2, a library, BIC Volume IO Library, which enables MINC interaction in C exists. The library supports the necessary ability to read and write MINC volumes as well as other types of general routine handling of MINC volumes. The library contains an amount of functions for handling and manipulation of MINC volumes, and they can easily be included in C.

5.5.1 Extraction of grey-level intensities

The functionality is implemented in a C program that takes a segmented CT image and the corresponding original CT image as inputs. The C program generally consists of one function, which is the main function. The main function generally consists of three for-loops, which are implemented like this:

```
for (voxel_z=0; voxel_z<masksizes[0]; voxel_z++)
for (voxel_y=0; voxel_y<masksizes[1]; voxel_y++)
for (voxel_x=0; voxel_x<masksizes[2]; voxel_x++)
```

The three for-loops ensure that each voxel in the segmented CT image is run through. An if-statement in the third for-loop examines whether the value of the voxel in the segmented CT image is above 0. To determine whether the voxels have a value above 0, the function `get_volume_real_value()` is applied on the specified voxel in the segmented CT image. If the value is above 0, it is a voxel that represents part of the lungs, and the grey-level intensity of the corresponding voxel in the original CT image is extracted by applying the `get_volume_real_value()` once again.

The extracted grey-level intensities are written to a text file. The number of outputs in the text file should correspond to the number of voxels with a value above 0 in the segmented CT image, which is the case for all images.

5.5.2 Texture features derived from image histogram-data

Texture features are derived by means of MATLAB®İn MATLAB® the text file is imported and the texture features can be derived with functions which are already defined.

5.6 Co-occurrence matrix

The co-occurrence matrix is set to express how often given pairs of voxels occur in the CT image. To compute a co-occurrence matrix, a search through the CT image should be conducted. The search needs to be defined by a displacement vector with a direction and a distance between the pairs of voxels which are evaluated, cf. Section 4.2.4. For volumetric data, 26 directions exist but only 13 of these are different [4]. In this project, the search in 13 different directions is conducted with one distance between the pairs of voxels which are evaluated. This distance is selected to be 1, i.e. it is a voxel and its neighbouring voxel in the given direction that constitute an evaluated pair of voxels. In Table 5.1, the 13 different directions are defined and listed by their corresponding displacement vector (d=(dx, dy, dz)), which defines the search through the image.

Displacement vector
(1, 0, 1)
(1, 0, 0)
(1, 0, -1)
(1, 1, 1)
(1, 1, 0)
(1, 1, -1)
(0, 1, 1)
(0, 1, 0)
(0, 1, -1)
(-1, 1, 1)
(-1, 1, 0)
(-1, 1, -1)
(0, 0, 1)

Table 5.1: The table shows the applied displacement vectors for the computation of co-occurrence matrices.

In general, a co-occurrence matrix is computed for each defined displacement vector. Texture features are derived for each co-occurrence matrix after which an average value for each texture feature is found. With 13 different directions and only one distance, 13 co-occurrence matrices should be computed for each CT image. As the data in this project consists of two CT images for 22 patients and each is divided into the left and right lung, 1144 co-occurrence matrices should be computed. In this project, a single co-occurrence matrix for each lung is computed however. It is assumed that entering all counts of how often given pairs of voxels, based on the displacement vector, occur in an image in one co-occurrence matrix, and deriving texture features for that single co-occurrence matrix is reasonable. The size of a co-occurrence matrix is determined by the range of grey-level intensities in the image. The grey-level intensities of each CT image are declared to lie in a range of 0 to 255 in order to make the computation of the co-occurrence matrix efficient. Hence, the size of the co-occurrence matrix is 256 x 256. To compute a co-occurrence matrix based on the above mentioned, the following should be conducted in all of the 13 directions:

- A segmented CT image and the corresponding original CT image should be taken as inputs.
- Each voxel with a value above 0 in the segmented CT image should be identified.
- The corresponding voxel in the original CT image should be identified and its value should be registered.
- The neighbouring voxel in the segmented CT image should be identified.
- The corresponding neighbouring voxel in the original CT image should be identified and its value should be registered.
- A count of a given distribution of grey-level intensities should be conducted and filled into the corresponding entry of the co-occurrence matrix.

This functionality is implemented in C for the same reasons as those stated in Section 5.5.

5.6.1 Computation of co-occurrence matrix

A C program, in which the functionality is implemented, has been written. The C program takes a segmented CT image and the corresponding original CT image as inputs, and generally consists of one function, which is the main function. In the main function, the co-occurrence matrix is declared and initialised as an array by `int Matrix[256][256]={{0}}`, i.e. the co-occurrence matrix initially consists of zeros. Additionally, the grey-level intensities are declared to be in a range of 0 to 255 by applying the function `set_volume_real_range()`.

In the main function, the 13 different directions are defined individually to ensure that a neighbour exists. Each direction is defined by three for-loops in accordance to their definition in Table 5.1. The for-loops ensure that voxels in the segmented CT image is run through in the correct direction, and that the content of the C program is initialised at the correct position. The for-loops are followed by an if-statement which examines whether a voxel value in the segmented CT image is above 0. This is determined by applying the function `get_volume_real_value()` on the given voxel. If the value is above 0, the voxel represents part of the lung, and the intensity of the corresponding voxel in the original CT image is set to `i` by applying the function `get_volume_real_value()` again. Subsequently using the same function, the neighbouring voxel in the segmented CT image is evaluated. If it has a value above 0, the corresponding voxel in the original CT image is set to `j`. This pair of voxels, (`i`,`j`), is then declared as integers `k` and `l` and their occurrence is registered in the co-occurrence matrix by `Matrix[k][l]++`. Hence, the entry (`k`,`l`) is counted one up. The pair of voxels is declared as integers as `Matrix` is declared integer and the intensity in the CT image is a float. This process is conducted for each voxel in the segmented CT image and for each direction. When the search through the CT image is finished, the co-occurrence matrix is written to a text-file.

5.6.2 Texture features derived from co-occurrence matrix

MATLAB® has an image processing toolbox that supports a set of functions usable for texture analysis. Thus, after computation of the co-occurrence matrix, the text file in which the matrix has been written is imported into MATLAB®.

To derive texture features, the co-occurrence matrix has to be symmetrical to include all 26 directions. A matrix is symmetrical when the same values occur in entries on opposite sides of the diagonal. A symmetrical matrix is obtained by transposing the co-occurrence matrix and add it to the original co-occurrence matrix. Also, the entries should be normalised by which they contain the joint probability occurrence of given voxel pairs, instead of counts. The texture features: contrast, correlation, energy, and homogeneity can be derived by using a predefined function in MATLAB®İt ensures automatically that the symmetrical co-occurrence matrix is normalised before texture features are derived.

Chapter 6

Evaluation of results

In this chapter, the results, i.e. the derived texture features, will be presented to determine which statistical test is most applicable. After presentation of the results, theory of the chosen statistical test is described before an actual test is conducted. The results are subsequently presented, and further evaluation is conducted by applying a discriminant analysis.

6.1 Presentation of derived texture features

In this presentation, the data is based solely on the lungs in which the tumour is located, since lung damage after radiation therapy is confined to that lung. The patients are divided into two groups, namely those without lung damage and those with lung damage. From the text files containing the extracted histogram-data, three texture features have been derived, i.e. mean, variance, and standard deviation. From the text files containing the co-occurrence matrices, four texture features have been derived, i.e. contrast, correlation, energy, and homogeneity. Box plots, showing each texture feature for both groups of patients, have been created and are presented in the following. A box plot shows the median (horizontal red line), the upper and lower quantiles (blue box), and the minimum and maximal values (called whiskers which are represented by vertical lines from either end of the blue box) of a data set. From a box plot it is possible to determine the skewness of the data. If the median is not placed centrally in the box then the data is skewed. This is also the case if one of the whiskers are much longer than the other. [28] In this project, the number of samples is too low to evaluate skewness. The number of samples is 14 for the group without lung damage and eight for the group with lung damage. Instead the tendencies between the baseline CT images and the follow-up CT images can be illustrated.

Box plot of mean

Figure 6.1 shows the box plot for the mean values. The two boxes to the left show the mean values from the group without lung damage for the patients' baseline and follow-up CT images, respectively. The two boxes to the right show the mean values for the group with lung damage for the patients' baseline and follow-up CT images, respectively. This setup with the groups and the baseline and follow-up CT images is the same for all following box plots. When looking at the group without lung damage (the two boxes on the left) the

range which the data lies within is clearly increased in the follow-up CT images compared to the baseline CT images. The opposite is the case when looking at the group with lung damage, where the range is almost decreased to half from the baseline CT images to the follow-up CT images. The range which the mean values lies within is in the lower range of all grey-level intensities which was expected since the lungs mostly consist of air, cf. Section 2.2.3.

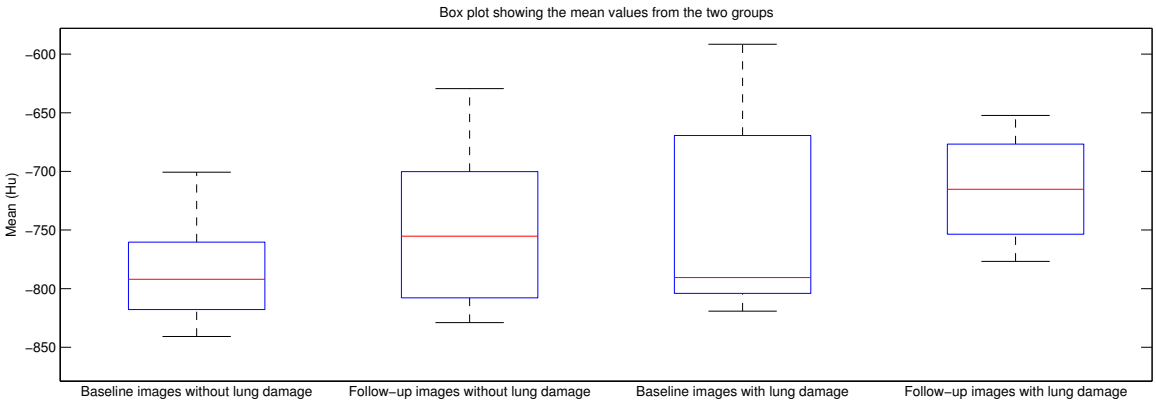

Figure 6.1: The figure shows the box plot of the mean values for the patients without and with lung damage.

Box plot of variance

Figure 6.2 shows the box plot of the variance values for the patients without and with lung damage. When looking at the group without lung damage (the two boxes on the left), the range which the data lies within is increased in the follow-up CT images. The range is approximately the same when looking at the group with lung damage. Instead the range within the upper and lower quartiles is more than doubled. The box plot of the standard deviation is not shown since it is identical with the box plot of the variance, due to the fact that the standard deviation is derived from the variance.

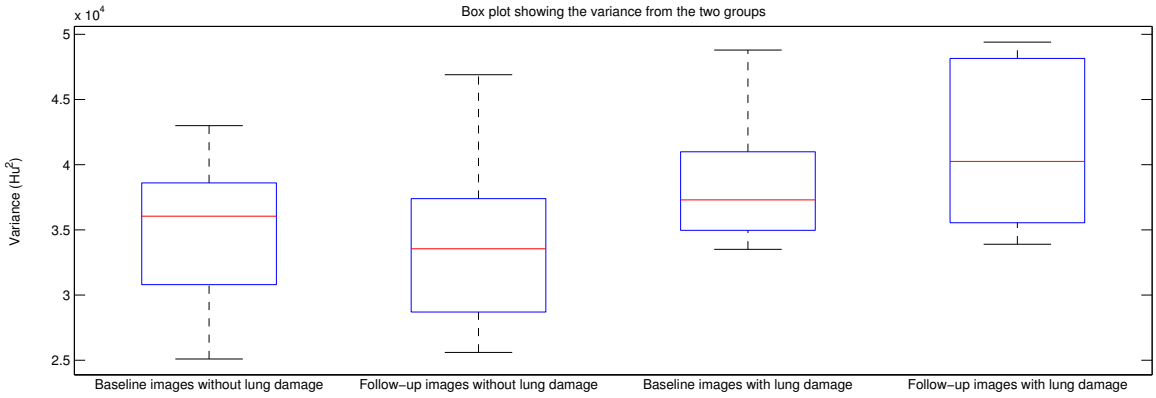

Figure 6.2: The figure shows the box plot of the variance values for the patients without and with lung damage.

Box plot of contrast

Figure 6.3 shows the box plot of the contrast values for the patients without and with lung damage. For both groups it is obvious that the range which the data lies within is decreased from the baseline CT image to the follow-up CT image. It should be noted that the two red crosses in the follow-up CT image from the group without lung damage indicate two outliers which deviate a lot from the rest of the data. From the box plot it is possible to determine that the contrast in the images is in the lower range meaning that the contrast does not vary much through the image which is expected since the lungs mostly consist of air, cf. Section 2.2.3.

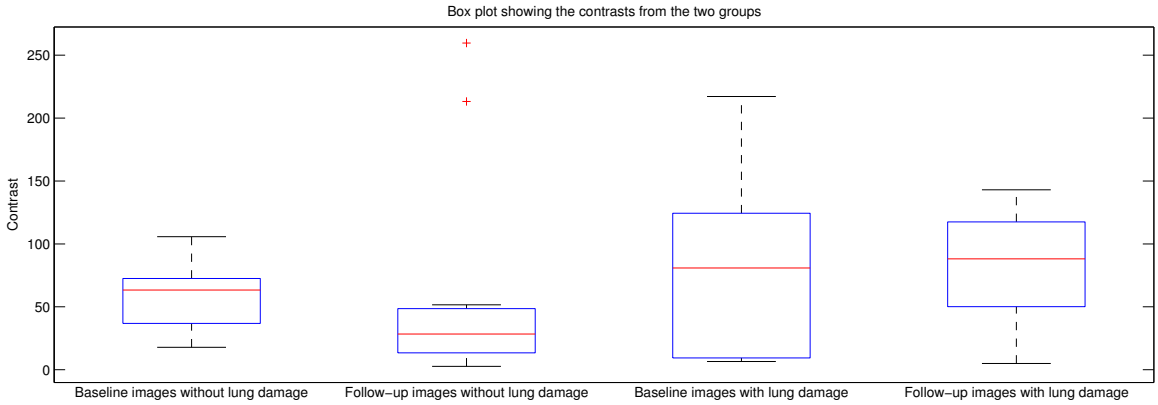

Figure 6.3: The figure shows the box plot of the contrast values for the patients without and with lung damage.

Box plot of correlation

Figure 6.4 shows the box plot of the correlation values for the patients without and with lung damage. For both groups the range which the data lies within clearly increases from the baseline CT images to the follow-up CT images. Again the red cross in the baseline CT image from the group without lung damage indicates an outlier which deviates a lot from the rest of the data. From the box plot it can be determined that the images are positively correlated since the correlation values lie in the positive range, cf. Section 4.2.4.

Box plot of energy

Figure 6.5 shows the box plot of the energy values for the patients without and with lung damage. When looking at the group of patients without lung damage the range which the data lies within is much increased from the baseline CT images to the follow-up CT images. There are two outliers in the baseline CT images and one in the follow-up images. In the group with lung damage the range which the data lies within is much decreased. In the follow-up CT images there is one outlier in this group. The range of the energy values are low when looking at the box plot, cf. Section 4.2.4. This indicates that the entries in the co-occurrence matrices are sparsely placed.

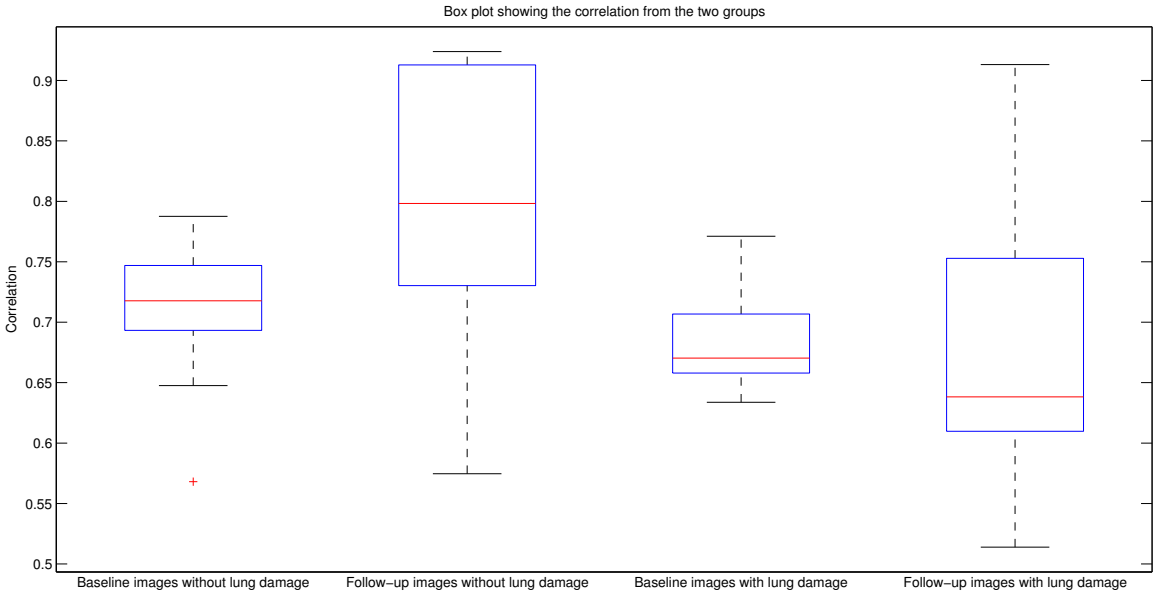

Figure 6.4: The figure shows the box plot of the correlation values for the patients without and with lung damage.

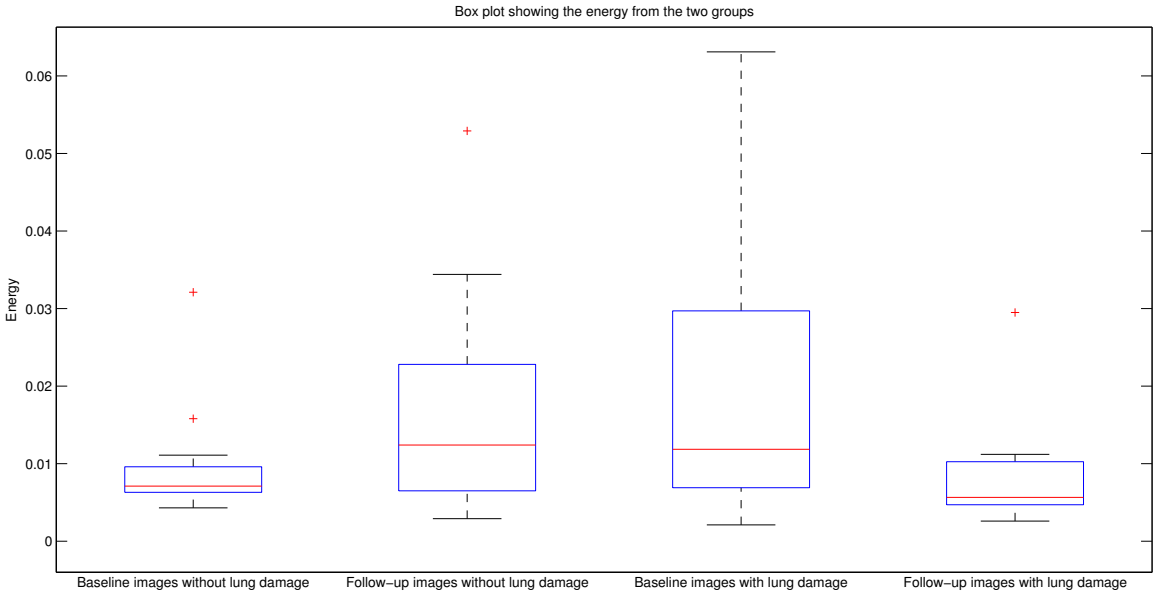

Figure 6.5: The figure shows the box plot of the energy values for the patients without and with lung damage.

Box plot of homogeneity

Figure 6.6 shows the box plot of the homogeneity values for the patients without and with lung damage. When looking at the group of patients without lung damage the range which the data lies within is increased from the baseline CT images to the follow-up CT images. But in the baseline CT images there are two outliers which affect the range to become smaller than if they were closer to the rest of the data. When looking at the group with lung damage the range which the data lies within is decreased between the baseline CT images and the follow-up CT images. One outlier is present in the follow-up CT images in the group with lung damage. The range of the homogeneity values lies in the middle of the possible range, cf. Section 4.2.4. This indicates that the entries of the co-occurrence matrices are not centered on the diagonal which would have been the case if the homogeneity was 1.

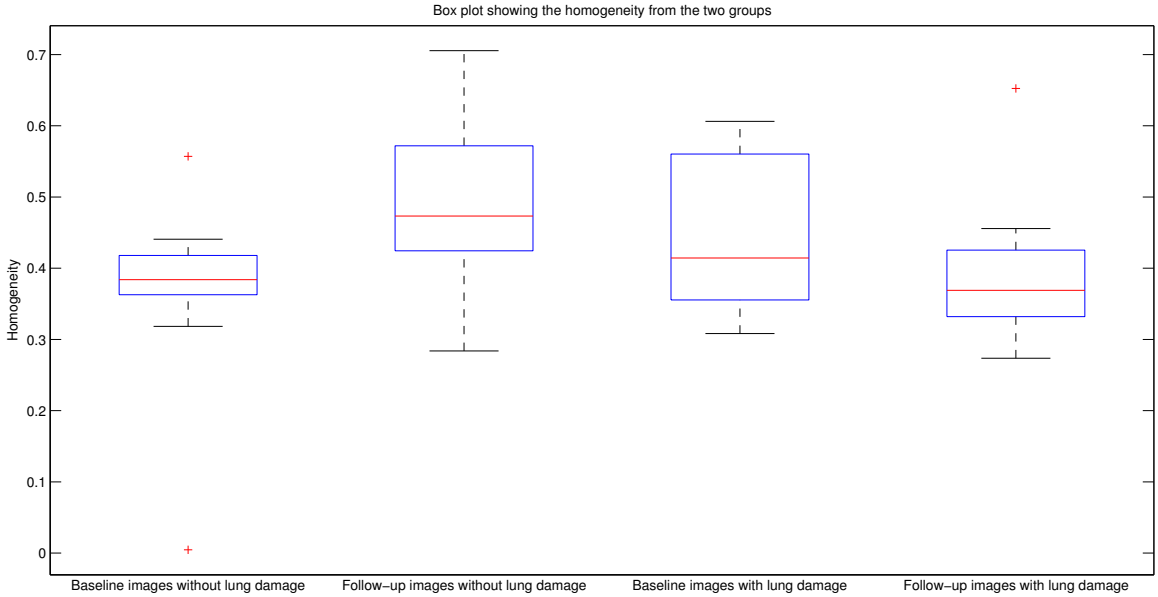

Figure 6.6: The figure shows the box plot of the homogeneity values for the patients without and with lung damage.

6.2 Theory of MANOVA

In this project, seven texture features are derived during texture analysis of each lung. Hence, a test statistic which is able to handle more variables (texture features) and more than one group is needed. When one variable in each of several groups is measured an analysis of variance (ANOVA) is applicable. The multivariate version of ANOVA is multivariate analysis of variance (MANOVA). With MANOVA it is possible to compare the means of the groups for each of the texture features, while maintaining the chosen magnitude of Type I error. Another advantage of MANOVA is its ability to consider the correlation between the multiple texture features which a series of ANOVAs is not able to do. [28]

In a MANOVA with two variables (X_1 and X_2) and k groups, the null hypothesis may be stated as:

$$H_0 : \mu_{11} = \mu_{12} = ... = \mu_{1k} \quad and \quad \mu_{21} = \mu_{22} = \mu_{2k} \tag{6.1}$$

where μ_{ij} denotes the mean of the variable i in group j. The H_0 says that the means of X_1 are the same for all k groups *and* the means of X_2 are the same for all k groups. The corresponding alternative hypothesis is:

$$H_A = \text{The } k \text{ populations do not have the same group means for } X_1 \\ \textit{and} \text{ the same group means for } X_2.$$

Thus, H_0 is rejected if any of the μ_{1j}'s are concluded to differ from each other *or* if any of the μ_{2j}'s are concluded to differ from each other. [28]

Several methods exist to test the MANOVA hypothesis. Often they result in the same conclusion or very similar conclusions regarding H_0 and they operate with similar power. In addition, they give identical results when only one variable is being analyzed or when the number of groups is two. In this project, MATLAB® is used, and it only contains one method to test the hypothesis in MANOVA, which is Wilks' Λ (capital greek lambda). Besides the number of groups in the project is two for which reason the other methods can be neglected. Hence, Wilks' Λ is the only method which will be described. Wilks' Λ is a quantity ranging between 0 and 1 and it is calculated with Equation 6.2:

$$\text{Wilks' lambda} = \Lambda = \frac{\mid \mathbf{W}_0 \mid}{\mid \mathbf{B}_0 + \mathbf{W}_0 \mid} = \prod_{i=1}^{p} \frac{1}{1+\theta_i} \tag{6.2}$$

where $\mathbf{W}_0$ is the within-group sum-of-squares and product matrix, $\mathbf{B}_0$ is the between-group sum-of-squares and product matrix, and θ_i are the eigenvalues of $\mathbf{W}_0^{-1}\mathbf{B}_0$. [21] H_0 is rejected for small values of Λ unlike most test statistics. In computer programs, Λ is often transformed to F or χ^2. Large values of F or χ^2 yield small p-values. [28]

MANOVA depends on certain assumptions which are important to be aware of. An important assumption is that the data represent random samples from the groups of interest and that the observations from each subject is independent. Another assumption is multivariate normality for each group of data. However, deviations from normality may have only a slight effect on Type I error rate. For example, MANOVA seems to be resistant to nonnormality due to skewness. MANOVA also assumes equal variances across all k groups and that the correlation between two variables must be the same in all k groups. [28]

6.3 Application of MANOVA

In this project, the observations for each subject are independent. Although each group of data is not normally distributed, it is not considered an issue since it only has a small effect on the Type I error. By arranging the results in different scenarios, different null hypotheses can be tested.

Scenario #1
To determine if a difference between the two groups (i.e. patients without and with lung damage) exists, a parameter that could be calculated is the difference between the baseline CT images and the follow-up CT images for each texture feature. With this scenario it is possible to test if there exists a difference in the baseline CT images and the follow-up CT images between the two groups, both in regard to the lungs containing the tumour and in

regard to the healthy lungs. The first test regarding the lungs containing the tumour, is the overall aim of the project. The second test is to see if there already exists a difference between the two groups in the healthy lungs, which could influence the results of the first test. In both cases the null hypothesis is as stated in Equation 6.1. When a MANOVA is applied with regard to all seven texture features at once, the resulting p-values are 0.1334 when testing on the lungs containing tumours and 0.1510 when testing on the healthy lungs. These results indicate that it is not possible to reject H_0 in either case, meaning that it is not possible to determine if there is a statistical difference between the baseline and follow-up CT images in the two groups. As the texture features are derived from two different methods of texture analysis, it is interesting if that influences the results. By dividing the data into two separate matrices, one containing the observations of the texture features derived from image histograms and one containing the observations of the texture features derived from the co-occurrence matrices, it is possible to determine if a difference exists between the two groups in these two scenarios. When only including the texture features derived from image histograms, p-values of 0.5607 and 0.1800 were obtained for the lungs containing tumour and the healthy lungs, respectively. Thus, it is not possible to reject H_0, indicating that it is not possible to observe a statistical difference between the baseline and follow-up CT images in the two groups. When including the texture features derived from co-occurrence matrices, p-values of 0.0527 and 0.0726 were obtained for the lungs containing tumour and the healthy lungs, respectively. These p-values are much lower, but it is still not possible to reject H_0. From these results it can be concluded that no statistical difference exists between the groups of patients without lung damage and the group of patients with lung damage. The results are identical for both the lungs containing tumour and the healthy lungs. However, the results implicate that the texture features derived from the co-occurrence matrices may be better at discriminating the two groups.

Scenario #2
Instead of examining the difference between the baseline CT images and the follow-up CT images from the two groups, it can be tested if a difference exists between the texture features of the baseline and follow-up CT images within the two groups. The null hypothesis is again as stated in Equation 6.1. When all the texture features are included in the group with lung damage, the p-values are 0.6547 and 0.7512 for the lungs containing the tumour and for the healthy lungs, respectively. This means that H_0 cannot be rejected. This is also the case if the texture features are divided into two, the texture features derived from the image histograms and the texture features derived from the co-occurrence matrices, respectively. The p-values are 0.5835 (lungs containing tumour) and 0.5560 (healthy lungs) with the three texture features derived from the image histograms. The p-values are 0.5645 (lungs containing the tumour) and 0.6154 (healthy lungs) with the four texture features derived from the co-occurrence matrices.

Scenario #3
When examining the group without lung damage, H_0 can be rejected when looking at both the healthy lungs (p-value of 0.0102) and the lungs containing tumour (p-value of 0.0293). In the lungs containing tumour this result is expected, since the tumour is shrunken or even disappeared in the follow-up CT images and no lung damage has developed. However it was not expected that H_0 could be rejected for the healthy lungs, since no statistical difference should be present in these lungs, and it does make the result regarding the lungs containing tumour questionable. For both the lungs containing tumour and the healthy lungs, the p-

values calculated from the texture features derived from the co-occurrence matrices (p-values of 0.0197 (lungs containing tumour) and 0.0051 (healthy lungs)) are much smaller than those calculated from the texture features derived from the image histograms (p-values of 0.2599 (lungs containing tumour) and 0.1042 (healthy lungs)). From the p-values it is possible to reject H_0 when they are calculated from the texture features derived from the co-occurrence matrices.

Scenario #4
The last scenario is to examine the healthy lungs in comparison with the lungs containing tumour. A difference is suspected since the texture features should be able to discriminate between a healthy lung and a lung containing tumour. Two MANOVAs are conducted, one for the group with lung damage and one for the group without lung damage. When examining the group with lung damage it is not possible to reject H_0 when all seven texture features are included (p-value of 0.1195). Again, if the texture features are divided in two, the p-value for the texture features derived from the image histograms is 0.0522 and the p-value for the texture features derived from the co-occurrence matrices is 0.5331. Examining the group without lung damage, the p-values are high in all three combinations of texture features. The p-value when all seven texture features are included is 0.8717. The p-values for the texture features derived from the image histograms and from the co-occurrence matrices are 0.4221 and 0.9776, respectively.

To summarize and give an overview of all the p-values they are displayed in the Table 6.1.

6.4 Discriminant analysis for further evaluation of results

In Section 6.3, a MANOVA test examined whether a statistical difference between patients with lung damage and patients without lung damage exists, based on the derived texture features. The result of the test was that no statistical difference between patients with lung damage and patients without lung damage exists. The results however implicated that the texture features derived from the co-occurrence matrices were best at discriminating the two groups of patients. It is thus chosen to examine whether the patients can be classified as having lung damage or not by conducting a discriminant analysis. In the discriminant analysis, *a priori* knowledge of which patients have lung damage is applied.

Discriminant analysis is a technique in which samples are classified into one of two or more predefined groups on the basis of multivariate samples. Compared to principal component analysis, which seek directions that are efficient for representation of data, discriminant analysis seek directions that are efficient for discrimination of data. The principle of discriminant analysis can be explained by considering the problem of projecting data from d dimensions onto an arbitrary line. Such projection will usually produce a mixture of samples from all of the groups and thus make the process of recognition difficult. Yet, if the line is moved, it may be possible to find an orientation for which the projected samples are well separated. [22] [3]

In discriminant analysis, different discriminant functions can be applied. The discriminant function specifies the process of discrimination, i.e. classification, which is conducted. The function can e.g. be linear or quadratic. In linear discriminant analysis, a multivariate normal density is fitted to each group with a pooled estimate of covariance, i.e. the covariances

Scenario	Description	p-values		
		All seven features	Three histogram features	Four co-occurrence features
#1	No lung damage vs. lung damage in regards to the difference between baseline and follow-up images (Tumour lungs)	0.1337	0.5607	0.0527
	No lung damage vs. lung damage in regards to the difference between baseline and follow-up images (Healthy lungs)	0.1510	0.1800	0.0726
#2	Baseline vs. follow-up images in the group with lung damage (Tumour lungs)	0.6547	0.5835	0.5645
	Baseline vs. follow-up images in the group with lung damage (Healthy lungs)	0.7512	0.5560	0.6154
#3	Baseline vs. follow-up images in the group without lung damage (Tumour lungs)	0.0293	0.2599	0.0197
	Baseline vs. follow-up images in the group without lung damage (Healthy lungs)	0.0102	0.1042	0.0051
#4	Healthy vs. tumour lungs from baseline images in the group with lung damage	0.1195	0.0522	0.5331
	Healthy vs. tumour lungs from baseline images in the group without lung damage	0.8717	0.4221	0.9776

Table 6.1: The table shows the tested scenarios and their corresponding p-value.

of the groups are identical. Linear discriminant analysis is the most common type of discriminant analysis. [3] In quadratic discriminant analysis, multivariate normal densities are fitted with covariance estimates stratified by the predefined groups. [21]

6.4.1 Classification of patients by discriminant analysis

In MATLAB® a function for discriminant analysis with different discriminant functions exists. A discriminant analysis by the means of this functions is conducted by dividing data into a test set and a training set. Additionally, to apply the function, the group to which samples from the training set belong should be defined. The output of the discriminant analysis is a class vector which contains the group to which each sample of the test set has been classified into.

In this project, discriminant analyses with different discriminant functions have been conducted, and the applied data was from Scenario #1 in regard to lungs containing a tumour.

The discriminant analysis is thus based on 8 patients with lung damage and 14 patient without lung damage. A sample, i.e. a patient, from the data was extracted and set to function as the test set, while the rest was set to function as the training set. Hence, each patient was tested and classified individually based on the training set. A linear discriminant function showed the best results. In Table 6.2, a confusion matrix with the result of the linear discriminant analysis is illustrated. In the confusion matrix, each column represents the occurrences in a classified class, whereas each row represents the occurrences in an actual class. Five out of eight patients with lung damage are classified correctly, while ten out of 14 patients without lung damage are classified correctly.

	Lung damage	No lung damage
Lung damage	5	3
No lung damage	4	10

Table 6.2: The table illustrates the results of the linear discriminant analysis with a confusion matrix. Each column represents the occurrences in a classified class, whereas each row represents the occurrences in an actual class.

Hence, by conducting a linear discriminant analysis about 68 % of the patients are classified correctly.

Chapter 7

Recapitulation

In this chapter, the applied methods to fulfill the aim of this project and the evaluation of the results will be discussed. Afterwards, a conclusion on this project will be presented.

7.1 Discussion

Themes and issues relevant for this project will be discussed in this section.

In this project, it was examined whether a difference between baseline and three month follow-up CT images could be determined, and thus enable a quantification of lung damage. In order to examine this, a texture analysis of the lungs was conducted, where seven texture features were derived for each lung. Hence, three of the seven texture features were derived from an image histogram and the remaining four texture features were derived from a co-occurrence matrix. In Section 6.3, when conducting multivariate analyses of variance (MANOVA) of the texture features in regard to patients with and without lung damage, different scenarios were examined. Scenario #1, examined the general aim of this project. Hence, whether a difference between baseline and follow-up CT images could be determined between the two groups of patients. The result of that MANOVA was that no statistical difference was detectable. The MANOVA however implicated that texture features derived from the co-occurrence matrices were better at discriminating between the two groups. For that reason, a linear discriminant analysis, based on texture features derived from the co-occurrence matrices, was conducted. The linear discriminant analysis was successful in classifying 68 % of the patients correctly. It could be assumed that more patient data available could be beneficial both in regard to the MANOVA and the linear discriminant analysis. Further investigations could be made to determine if more or if different texture features should be derived from the texture in the lungs. Other texture features may be better at characterising the texture of the lung tissue.

An unexpected result was that the MANOVA showed a statistical difference between baseline and follow-up CT images when examining healthy lungs in patients without lung damage. This result was interesting as a difference was not expected due to the fact that it is healthy lungs which was assumed not influenced by the radiation therapy. The results makes the other results questionable. More patient data available may be able to correct such a result.

Several segmentation methods and approaches to how a texture analysis can be conducted exist. The chosen methods and approaches in this project could be examined as well. The chosen method for segmentation of the lungs was region growing. Region growing is a simple segmentation method and a function in MINC could conduct such region-based segmentation. The method is user-dependent as visual inspection regarding intensities and localisation of the lungs is necessary to initialise the growing process. Furthermore, the method requires determination of which interval of intensities the growing process should be conducted. As the lungs are seen as dark regions in the CT images initialisation of the growing process is straightforward. Observations made with regard to the segmentation showed acceptable results. Minor leakages to the surrounding tissues were observed in a couple of CT images but either it was concluded that the leakage was minimal or the relevant patient was excluded from the project. Large tumours were sometimes not included in the segmentation and since the tumour shrunk in the follow-up CT image, causing more lung tissue to be included in the segmentation, it would probably affect the texture analysis and thereby the presumed difference between the baseline and the follow-up CT images. Another factor resulting from the segmentation and which may influence the results is the inclusion of the airways within the lungs. This factor was neglected since the airways were included in both the baseline and the follow-up CT images, but it should still be examined to determine whether it has an influence. The manual division of the segmented lungs into right and left, was not always perfect. A different segmentation may correct this uncertainty.

In regard to the computation of the co-occurrence matrices, several different approaches could have been chosen, which may influence the results. Generally, a co-occurrence matrix is computed for each direction and length of the displacement vector. A texture analysis in which co-occurrence matrices are computed can thus easily become very comprehensive. In this project, it was chosen to incorporate all 26 directions, which exist in volumetric data, in one matrix. The decision was based on the fact that in other studies they averaged the texture features derived from different co-occurrence matrices based on a single direction. The chosen approach was thus found to be acceptable. In other studies, different lengths of the displacement vector were included in the texture analysis, but since no reasonable argument was given to which length was the best, a length of 1 was chosen in this project. Further analysis should be conducted to determine whether another length would be more suitable. Another approach could be to divide the lung further instead of characterising the whole lung. It is an approach that is often used in texture analysis to determine where in an image the texture features differ. Also, in regard to this project, it is assumed to be beneficial to solely conduct the texture analysis within the field of irradiation as the lung damage occur in that area. If the field of irradiation had been given, the CT image volume could have been reduced significantly.

All of the above states areas which need further investigation before texture analysis should be disregarded to enable quantification of lung damage. Also, an important aspect to note is that not a lot of studies have been conducted where texture analysis is used to characterise the texture of the lungs. More often texture analysis has been used in segmentation of the lungs. When texture analysis has been used to characterise medical images, it has not been possible to find instances where it has been used to characterise the difference between two images from the same patient.

7.2 Conclusion

The aim of this project was to develop a method which enables quantification of lung damage caused by NSCLC treatment with radiation therapy, using baseline and three month follow-up CT images.

Different methods of image analysis were applied to fulfil the aim of this project, resulting in main phases which involved a segmentation of the lungs by region growing, a texture analysis of lung tissue during which texture features from image histograms and co-occurrence matrices were derived, and an evaluation of results.

Based on the evaluation of results, a statistical difference between patients with lung damage and patients without lung damage could not be found. The MANOVA implied, however, that the texture features extracted from the co-occurrence matrices were better at characterising the lung tissue in the two groups of patients than the texture features derived from the image histograms. In this project, different issues can be further investigated in regard to segmentation and computation of the co-occurrence matrices. When considering all the aspects mentioned in Section 7.1, texture analysis should not be completely disregarded in quantification of lung damage between patients with and without lung damage. Some of the aspects that could be pointed out are more patient data, different or more texture features, and a different segmentation that is able to distinguish between the left and the right lung.

Bibliography

[1] McConnell Brain Image Center, April 2011. `http://www.bic.mni.mcgill.ca/ServicesSoftware/MINC`.

[2] Mesothelioma cancer and lung disease, May 2011. `http://www.mesotheliomalungs.org/radiation-therapy-mesothelioma-and-cancer`.

[3] Richard O. Duda, Peter E. Hart, and David G. Stork. *Pattern Classification*. John Wiley and Sons, Inc., 2. edition, 2001.

[4] Arati S. Kurani et al. Co-occurrence matrices for volumetric data. *International Conference on Computer Graphics and Imaging*, 2004.

[5] David A. Palma et al. A new approach to quantifying lung damage after stereotactic body radiation therapy. *Acta Oncologica*, 50:509–517, 2011.

[6] Feng-Ming Kong et al. Final toxicity results of a radiation-dose escalation study in patients with non-small-cell lung cancer (NSCLC): Predictors for radiation pneumonitis and fibrosis. *International journal of radiation oncology biology and physics*, 65(4):1075–1086, 2006.

[7] Frank V. Fossella et al. *Lung Cancer*. Springer, 2002.

[8] G. Castellano et al. Texture analysis of medical images. *Clinical Radiology*, 59:1061–1069, 2004.

[9] Ian Hunt et al. *ABC of Lung Cancer*. Blackwell Publishing Ltd, 1. edition, 2009.

[10] Jerrold T. Bushberg et al. *The essential physics of medical imaging*. Lippincott Williams and Wilkins, 2. edition, 2002.

[11] Jianhua Yao et al. Computer-aided Diagnosis of Pulmonary Infections Using Texture Analysis and Support Vector Machine Classification. *Academic Radiology*, 18:306–314, 2011.

[12] K. M. Fong et al. Molecular biology of lung cancer: clinical implications. *Thorax*, 58:892–900, 2003.

[13] Kyung Joo Park et al. Radiation-induced lung disease and the impact of radiation methods on imaging features. *RadioGraphics*, 20(1):83–98, 2000.

[14] Robert M. Haralick et al. Textural Features for Image Classification. *IEEE Transactions on Systems, and Cybernetics*, 3(6):610–621, 1973.

[15] Sandra McDonald et al. Injury to the lung from cancer therapy: clinical syndromes, measurable endpoints, and potential scoring systems. *International journal of radiation oncology biology and physics*, 31(5):1187–1203, 1995.

[16] Vassili A. Kovalev et al. Three-Dimensional Texture Analysis of MRI Brain Datasets. *IEEE Transactions on Medical Imaging*, 20(5):424–433, 2001.

[17] Zhen Ma et al. A review of algorithms for medical image segmentation and their applications to the female pelvic cavity. *Computer Methods in Biomechanics and Biomedical Engineering*, 13(2):235–246, 2009.

[18] Rafael C. Gonzalez and Richard E. Woods. *Digital Image Processing.* Pearson, 3. edition, 2008.

[19] Radiation Therapy Oncology Group, May 2011. `http://www.rtog.org/ResearchAssociates/AdverseEventReporting/AcuteRadiationMorbidityScoringCriteria.aspx`.

[20] Willi A. Kalender. *Computed Tomography.* Publicis Corporate Publishing, 2. edition, 2005.

[21] W. J. Krzanowski. *Principles of Multivariate Analysis - A User's Perspective.* Oxford Science Publications, 1988.

[22] P. A. Lachenbruch and M. Goldstein. Discriminant Analysis. *Biometrics*, pages 69–85, 1979.

[23] David MacDonald, January 2011. `http://www.bic.mni.mcgill.ca/~david/`.

[24] Orla McArdle and Deidre O'Mahony. *Oncology - An illustrated colour text.* Churchill Livingstone Elsevier, 2008.

[25] World Health Organization, February 2011. `http://www.who.int/mediacentre/factsheets/fs297/en/`.

[26] Steven W. Smith. *The Scientist and Engineer's Guide to Digital Signal Processing.* California Technical Publishing, 1. edition, 1997.

[27] Robert Souhami and Jeffrey Tobias. *Cancer and its management.* Blackwell Publishing Ltd, 5. edition, 2005.

[28] Jerrold H. Zar. *Biostatical Analysis.* Pearson, 5. edition, 2010. ISBN-10: 0-13-206502-9,ISBN-13: 978-0-13-206502-3.